QUARTERLY PROGRESS REPORT FOR MTR-ETR TECHNICAL BRANCHES
First Quarter - 1958

Edited by R. G. Fluharty

September 2, 1958

AEC RESEARCH AND DEVELOPMENT REPORT
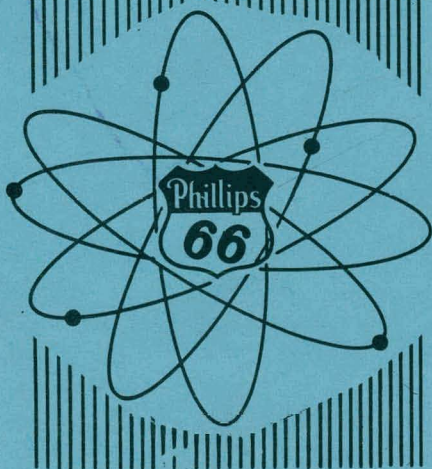
Phillips 66

PHILLIPS PETROLEUM CO.
ATOMIC ENERGY DIVISION
(UNDER CONTRACT NO. AT (10-1)-205)

IDAHO OPERATIONS OFFICE
U. S. ATOMIC ENERGY COMMISSION

DISCLAIMER

This report was prepared as an account of work sponsored by an agency of the United States Government. Neither the United States Government nor any agency Thereof, nor any of their employees, makes any warranty, express or implied, or assumes any legal liability or responsibility for the accuracy, completeness, or usefulness of any information, apparatus, product, or process disclosed, or represents that its use would not infringe privately owned rights. Reference herein to any specific commercial product, process, or service by trade name, trademark, manufacturer, or otherwise does not necessarily constitute or imply its endorsement, recommendation, or favoring by the United States Government or any agency thereof. The views and opinions of authors expressed herein do not necessarily state or reflect those of the United States Government or any agency thereof.

DISCLAIMER

Portions of this document may be illegible in electronic image products. Images are produced from the best available original document.

QUARTERLY PROGRESS REPORT FOR MTR-ETR TECHNICAL BRANCHES

First Quarter 1958

Edited by R. G. Fluharty

Previous Quarterly Reports in This Series

PHILLIPS PETROLEUM COMPANY
Atomic Energy Division

Under Contract
AT(10-1)-205
to

IDAHO OPERATIONS OFFICE
U. S. ATOMIC ENERGY COMMISSION

THIS PAGE

WAS INTENTIONALLY

LEFT BLANK

TABLE OF CONTENTS

TABLE OF CONTENTS - CONTD

LIST OF FIGURES

LIST OF TABLES

LIST OF TABLES - CONTD

QUARTERLY PROGRESS REPORT FOR MTR-ETR TECHNICAL BRANCHES

First Quarter 1958

Edited by R. G. Fluharty

Work Directed by: D. R. deBoisblanc, Director, Reactor Physics and
Engineering Branch
W. B. Lewis, Director, Theoretical Physics and
Applied Mathematics Branch
J. E. Evans, Director, Nuclear Physics Branch

I. SUMMARY

MTR Technical Assistance - Heat generation calculations showing a breakdown of U^{235} fission energy in the MTR has been completed giving 198 ± 6 Mev per fission. Calculations indicate the necessary control system changes to allow MTR operation with Pu^{239} as fuel. New shim rod magnets have been installed and one regulating rod has been changed to a metal sprayed type.

ETR Technical Assistance - Nondestructive methods of fuel and boron analysis for ETR fuel have been developed, and core measurements have been made using the new "pinned" plate elements which will receive full water flow. By placing large boron content elements in the center and low content on the outside a long burnout core with fairly uniform heat generation is achieved. Transient power studies have been used to demonstrate safety of the control magnet design. The regulating rod control system has been studied and recommendations made for modifications to improve operation.

Reactor Physics and Engineering - Transfer function analysis of heat exchangers using a space dependent differential equation for the heat exchanger is being applied to a system similar to the ETR for comparison with analyses using a lumped exchanger. Out-of-pile experiments are outlined to study metal-water reactions and initial results described. Thorium irradiation calculations and U^{233} build up measurements are summarized. RMF control element modifications allow direct reading to 1×10^{-7} δk/k.

Hydraulic and static testing of MTR production fuel assemblies has been made giving flow vs pressure drop, maximum flow rate at failure, and deflection to static pressure. The new elements did meet tentative minimum specifications, although they appear somewhat inferior to earlier elements. Hydraulic tests of tubular-type fuel elements are under way and a transparent variable-channel flow fixture is now available for direct observation of the flow. The program of irradiating various fuel plates is now under way with 19 of the 21 compositions on hand. Twelve compositions are currently being irradiated with 28% burnup and will continue to 40%. Pre-irradiation testing of the remaining fuel plates is in progress, and post-irradiation testing is scheduled for June.

Nuclear Physics - The U^{233} cross section measurements are continuing. Total-minus-fission cross section subtractions, eta, and fission product mass asymmetries data have been obtained. Preparations for gas scintillation fission counting are in progress, and total cross sections of Nd, Sm, Gd, and Pu^{240} have been submitted for the cross section compilation. Initial scattering measurements (10 to 150 ev) on W have been made. The low energy neutron velocity selector consisting of two phased rotors is under active development, and initial experimental results using a spinning sample technique are presented. Calculations of the gamma-ray detection efficiencies of different shapes of NaI crystals and extended sources have been completed, and a 4.7 millisecond isomer in Pb^{205} has been discovered. A description is given of the multichannel pulse height analyzer temporary storage system which is being developed.

II. MTR TECHNICAL ASSISTANCE

A. Heat Generation and Distribution in the MTR (R. A. Grimesey)

A breakdown of the U^{235} fission energy and its distribution in the MTR has been made and is reported in IDO-16443.[1] The calculations are made specifically for the MTR with a 3 x 9 loading and 40 Mw operation. The average energy generated per fission is found to be 198 ± 6 Mev of which ~90% is generated in the fuel plates.

The study was requested since a discrepancy has been observed between the measured heat generated by the MTR, as measured from the temperature rise and flow of the cooling water, and the calculated heat from fuel and flux distributions. As expected, the heat generated per fission is in essential agreement with the numbers used in the flux-fuel calculations. Since the flux-fuel calculations estimate 40 to 60% more heat than is measured, the possible 1.5% change, indicated for the energy per fission, makes an insignificant change in the calculated values.

The problem of determining the generation and distribution of heat in the MTR is resolved into three essential parts: (1) determination of direct fission energy, (2) determination of energy liberated from parasitic capture processes in the core and reflector, and (3) determination of the distribution of heat in the core and reflector. Tabular summaries of these considerations are given in Tables II-1, II-2, and II-3, respectively.

TABLE II-1

Breakdown of Direct Fission Energy as Given by Four Current Sources

Source	Glasstone, Edlund (Mev)	R. L. Murray (Mev)	Reactor Handbook CRR-489 (Mev)	CRP-642A (Mev)
	(1952)	(1956)	(1952)	(1956)
KE of Fission Fragments	162	167	168 ± 5	167.1 ± 2
KE of Fast Neutrons	6	5	5 ± 0.5	5 ± 0.5
Prompt Gamma-Rays	6	7	4.6 ± 1	7 → 12
Fission Product Gamma-Rays	5	6	7.5 } ± 2	7.5 } ± 2
Beta Decay Energy	5	5	5.5 }	5.5 }
Total	184	190	191 ± 8.5	192.1 + 9.5 - 4.5

(1) R. A. Grimesey, An Estimate of the Heat Generation and Distribution in the MTR, IDO-16443, (1958).

TABLE II-2

Generation of Heat Energy in the MTR

Event	Event per Fission	Energy per Event (Mev)	Class*	Energy per Fission (Mev)
Fission	1.	190 ± 8		190 ± 5.5
U^{235} Capture	0.182	6.4**	2	1.17
Al Capture	0.077	7	1	0.54
H_2O Capture	0.19	2.2	1	0.42
Xe Capture	0.058	10	2	0.58
Sm Capture	0.0117	8.4	2	0.1
Reflector				
H_2O Capture	0.272	2.2	1	0.6
Be Capture	0.528	6.8	1	3.6
Be (n,2n) Reaction	≈ 0.08	3.67	1	≈ 0.43
Neutrons that Escape Tank	0.15			≈ 0.1
Total	2.47 + 0.08 (n,2n)			197.5 ± 6

*Class 1 gamma-rays are those in which one photon possesses the total energy of a ground state transition. Class 2 gamma-rays are those in which the emission energy is scattered among many photons.

**The average energy per photon is ≈ 3 Mev.

TABLE II-3

Distribution of Heat in the MTR

Heat Source	Fuel Element (Mev/Fiss)	Moderator (Mev/Fiss)	Reflector (Mev/Fiss)	Escape to Graphite (Mev/Fiss)	Total (Mev/Fiss)
Fission Fragment	167				167
Fast Neutrons	0.5	2.9	1.4 + .13 Be(n,2n)	.1	5
β Energy	4	≈1			5
Primary γ Energy	5.7	5	4.9	.2	15.8
(n,γ) Energy in Reflector	0.4	0.3	3	.5	4.2
Be (n,2n)	0.05	0.04	0.30	.04	0.43
Total	177.7	9.24	9.7	.84	197.5

B. Xenon Override Computer Program (R. W. Goin)

A program has been completed for the IBM-650 to be used to determine the maximum number of fuel assemblies which can be carried over from the preceding charge. This will allow the MTR to go critical at a particular time after shutdown. The program utilizes Eq. (25) of IDO-16401[2] where the derivation, a discussion, and results are reported for the equation. Other discussions of fuel load calculations have been presented in IDO-16394[3] and IDO-16430.[4]

C. Special Fuel Experiments in the MTR

The second of a series of full core loadings of various nuclear fuel systems in the MTR is in preparation. The previous experiment using 20% U^{235} enriched uranium fuel is reported in IDO-16459.[5] The present experiment to

(2) H. L. McMurry, G. A. Cazier, R. W. Goin, Calculation of MTR Fuel Charges, IDO-16401, (1957).

(3) H. L. McMurry, Quarterly Progress Report for MTR Technical Branches, Second Quarter - 1957, IDO-16394, 20-8.

(4) H. L. McMurry, G. A. Cazier, and R. W. Goin, Quarterly Progress Report for MTR-ETR Technical Branches, Third Quarter - 1957, IDO-16430, 21-4.

(5) D. R. deBoisblanc and R. S. Marsden, Preliminary Evaluation of the 20% Enriched Uranium Core for the Materials Testing Reactor, IDO-16459, (1958).

be undertaken will employ Pu^{239}-aluminum alloy clad in aluminum in an array of 23 elements and 4 fuel shim rods in the standard 3 x 9 north slab loading of the MTR. Critical size calculations have been made,[6] and a summary report is being prepared.

1. **Control System Changes for Pu^{239} Load** (W. J. Byron, H. W. Davis)

Investigations of the control and safety aspects of the proposed Pu^{239} load have been conducted. These were required because of the differences in delayed neutron lifetimes and the value of β_{eff} (the yield of delayed neutrons) from those of the U^{235} loading in the MTR. Calculated analysis of the kinetics of the Pu loaded MTR revealed the maximum worth of the regulating rod and the maximum k addition rate (rod drive speed) permissible. The reactivity design specification is that the MTR regulating rod for Pu must be less than 0.2% $\delta k/k$.

All components for the control and safety systems modification are ready for use. A special regulating rod has been fabricated for the Pu core. The rod, as constructed, is mechanically identical to the MTR regulating rods used with U^{235} except that there is considerably less cadmium in the rod. An experiment with a dismantled regulating rod in the RMF provided information from which the final amount of cadmium was established.

Motors (900 rpm or half-speed) to drive the shim rods for the Pu core loading have been modified and are stored for later use with the experimental core. Half-speed motors were selected so as to keep the runaway reactor period (on high-speed withdrawal) high enough that the existing safety system can override it. Preliminary "safe-side" calculations indicate that the maximum period for this motor speed is 1/22 second. The corresponding period for normal U^{235} operation is 1/15 second with full speed motors. The safety scram system operates within 1/30 second. To adjust the Pu^{239} control system period to 1/15 second would require a $10,000 drive system in contrast to the $700 cost of the present motor. Refined calculations are under way to investigate power transients for this control system.

D. **MTR Developments**

1. **Shim Rod Magnet** (H. W. Davis)

All MTR shim rods are now completely equipped with magnets of the new cylindrical design.[7,8] The replacement was necessitated by the increased maintenance costs of the original magnets and also by the difficulty

(6) W. B. Lewis and G. O. Marshall, Quarterly Progress Report for MTR-ETR Technical Branches, Fourth Quarter - 1957, IDO-16436, 11.

(7) H. W. Davis, Quarterly Progress Report for MTR-ETR Technical Branches, Third Quarter - 1957, IDO-16430, 20-1.

(8) H. W. Davis and W. J. Byron, Quarterly Progress Report for MTR-ETR Technical Branches, Fourth Quarter - 1957, IDO-16436, 23.

experienced in obtaining replacement parts for the previous magnets. The new cylindrical magnet is manufactured at the MTR, hence, no replacement parts problem is expected to arise.

A measurement of the gamma dose received by the magnets for one cycle has been completed. Silver activated glass dosimeters were placed on top of the magnets, irradiated, and read after one cycle. The total dose registered by the dosimeters was 1.1×10^5 roentgen. This information indicates that insulators of the new highly cross-linked polyethylene now commercially available will last many cycles. Measurements of brittleness, conductivity, and other properties after irradiation also bear out this conclusion.

2. Sprayed Regulating Rod Calibration (W. J. Byron, H. W. Davis)

One of the regulating rods in the MTR has been changed to a diameter smaller than the original rods and the cadmium and stainless steel have been metal-sprayed on the rod. This type of fabrication should eliminate distortions occurring in previous rods, made by metal plate cladding of the cadmium strips onto the stainless steel rod, when water gets between the cadmium and stainless steel.

Calibration of this regulating rod by the period technique showed an initial reactivity for the rod of 0.3% δk/k. Periodic calibration of the rod will be made to establish the optimum life of the rod in the MTR.

3. Shim Rod Modifications (E. H. Porter)

Design continued on a shim rod embodying removable fuel and poison sections.[9] Engineering work was completed and flow rate and pressure drop calculations were made based on the new configuration. As presently envisioned, the fuel section of 16 curved plates will not be reversible. This decision was made when it became apparent that the gains derived from inverting the fuel section did not balance the engineering and fabrication complications. The poison section will be reversible, end for end, for increased service. Detailed construction drawings for the shim rod are being made.

(9) K. V. Moore and E. H. Porter, Quarterly Progress Report for the MTR Technical Branches, Second Quarter - 1957, IDO-16394, 34.

III. ETR TECHNICAL ASSISTANCE

A. ETR Critical Facility

1. Fuel Element U^{235} and Boron Content Analysis

   a. Reactivity Measurements (J. W. Henscheid)

   Because of the unpredictable variations in the boron content of the ETR fuel assemblies, it was deemed advisable to develop a nondestructive method of fuel and boron analysis. Reactivity measurements, as a means of determining the boron content in ETR elements, have been previously described.[10] These measurements indicated that the boron content varied widely from element to element and that, in general, it was considerably higher than that reported by Babcock and Wilcox (B & W), nominally 1.6 grams. Similar measurements have since been made on a number of ETR fuel elements from several different B & W shipments. The results of these measurements are tabulated in Table III-1 along with the B & W reported values. It should be pointed out that the boron content values from ETRC measurements are really "apparent content" values since segregation of the boron in the fuel plates could cause considerable self-shielding. It has been shown that segregation does exist;[11] therefore, the values reported here are undoubtedly low. However, these values do represent the equivalent effectiveness in a new loading.

TABLE III-1

Boron Content of ETR Elements

Fuel Element Number	ETRC Measured Values Boron Content (g)	B & W Reported Values Boron Content (g)	Fuel Content (g)
L338	1.83	2.597	237.46
L340	1.30	2.569	239.66
H301	2.20	1.144	256.29
H347	2.33	1.313	256.78
H352	2.24	1.547	255.57
H446	1.23	1.213	255.94
H499	0.98	1.217	254.36
H506	0.78	1.216	254.10
H528	0.75	1.226	255.73
H547	1.35	1.216	256.83

(10) D. L. Parry, Quarterly Progress Report for MTR-ETR Technical Branches, Third Quarter - 1957, IDO-16430, 8.

(11) F. H. Tingey, Quarterly Progress Report for MTR-ETR Technical Branches, Third Quarter - 1957, IDO-16430, 28.

In the measurements above, it was assumed that the fuel content in all of the "H" elements (nominally 255 grams of U^{235}) was constant and that the difference in reactivity effects between elements was not due to variations in fuel content. The validity of this assumption was borne out by subsequent reactivity measurements on five special fuel elements. These elements are identical to the standard "H" elements except that they contain no boron. The maximum deviation from the average of these five elements was equivalent to 1.3 grams U^{235}. This, however, is within the average experimental error in this type measurement.

The sensitivity (statistical weight) of boron in the vicinity of the core where these measurements were made is about 50 times that of U^{235}, when expressed in grams. Consequently, by making the assumption that the U^{235} content is the same in all fuel elements, the expected maximum error in the apparent boron content would only be about 0.03 grams. However, the experimental procedure used in obtaining the data in Table III-1 included additional uncertainties which, when critically evaluated, resulted in assigning maximum deviation limits of $\pm$ 0.1 gram to all values.

Recently a modified and more refined procedure has been used to measure the boron content in fuel elements. A known amount of natural boron (boron impregnated polyethylene tape) was uniformly loaded into one of the special fuel elements free of boron. This loaded element was placed in a selected grid position in the ETRC core, and the shim position for criticality was recorded. By varying the amount of boron in this element, a curve relating critical shim position to boron content was obtained. Subsequently, each of a selected group of 21 new pinned-type borated elements (Section III-A-2) were alternately placed in the selected grid position. The shim position for criticality was recorded in each case. Using the curve described above, the boron content of each of the elements was determined. It should be noted that this method of measuring boron content, in contrast to the previous method, is independent of (1) reactor period measurements, (2) the inhour relationship of period to reactivity, and (3) a shim rod calibration.

The values obtained using this method are shown in Table III-2 along with the B & W reported values. The maximum limits of error (due primarily to nonreproducibility) are approximately $\pm$ 0.04 gram. A cursory examination of Table III-2 shows that the variation in boron content is not a random effect. The content in the H^{560}'s is relatively constant, increases through the H^{570}'s and H^{580}'s, decreases again through the H^{590}'s to a low value in the upper H^{600}'s. On the basis of these observations, the boron content in each of the 30-some remaining pinned-type elements was estimated.

2. ETR Cycle 1 Core Measurements

ETR fuel elements have been received which will operate at the required water velocity for full power operation (175 Mw). The maximum power of the ETR has been limited to 90 Mw because of the inability of the elements to receive full water flow velocities. This limitation has been attributed to ripples in the fuel plates which set up differential pressures

in adjacent coolant channels.[12] Since the ripples were created during the brazing process, the effect has been eliminated by pinning the plates into the side plates.

TABLE III-2

Boron Content of ETR Elements

Fuel Element Number	ETRC Measured Values Boron Content (g)	B & W Reported Values Boron Content (g)	Fuel Content (g)
H563	1.34	1.548	255.17
H564	1.29	1.548	255.17
H565	1.32	1.548	255.17
H566	1.33	1.548	255.17
H567	1.36	1.548	255.17
H568	1.36	1.548	255.17
H569	1.36	1.548	255.17
H571	1.22	1.548	255.17
H574	1.73	1.552	254.45
H579	1.64	1.552	254.45
H581	1.74	1.552	254.45
H585	1.91	1.551	254.62
H590	1.44	1.553	254.32
H595	1.35	1.549	254.84
H601	1.11	1.552	254.90
H608	0.98	1.549	255.18
H609	0.78	1.548	255.14
H611	0.95	1.548	255.14
H614	0.75	1.553	255.06
H620	0.78	1.555	255.52
H625	0.76	1.555	255.52
Average	1.26		

A full loading of these "pinned" plate elements has been received and will be used in the ETR loading for Cycle 1 (previous cycles have been designated A through D). Criticality measurements have been performed in the ETRC for two loading arrangements using these elements.

(12) J. R. McGeachin and A. W. Brown, Quarterly Progress Report for MTR Technical Branches, Second Quarter - 1957, IDO-16394, 31.

a. Loading Arrangements and Control Rod Worth (T. K. DeBoer,
B. L. Hanson)

Because of the large variation in the boron content of the fuel
elements, (see Section III-Ala) it was possible to obtain a number of loading
arrangements that would produce the same control rod pattern at the beginning
of the cycle. It was decided to determine what the extreme core loadings
would be, and it was these two core loadings that were studied. In the
initial loading, the low boron content elements were placed in the center
grid positions, while those with high boron content were placed around the
outside. This loading contained 51 fuel elements (Fig. III-1). The second
loading arrangement contained 54 fuel elements (Fig. III-2) and was essentially
the initial core loading "turned inside-out" with the high boron elements
moved to the inside and the low boron elements to the outside.

The worth of No. 7 control rod (ETRC operational rod) was deter-
mined for both cores and was found to be 2.3% δk/k and 1.6% δk/k for the 51
and 54 element loadings, respectively. Since No. 13 rod is the rod with
which criticality is attained in the ETR rod program, its worth was also
determined for the 54 element core. It was measured to be 2.5% δk/k.

The 54 element core was chosen as the core arrangement to be used
in the ETR for the following reasons: (1) a more uniform heat generation
distribution is achieved by having the high boron elements in the center and
(2) the 54 element core will have a longer core life due to the additional
amount of fuel present in the three extra fuel assemblies.

b. Excess Reactivity (B. L. Hanson)

The controlled excess reactivity at start-up of the 54 element
core was measured by the distributed poison method. The poison introduced
was powdered metallic boron impregnated in extruded polyethylene tape.
Chemical analysis has indicated a uniform boron distribution and an average
boron content of 4.52 weight percent (w/%) and 0.998 w/%. Four 4.52 w/%
and three 0.998 w/% tapes were inserted into each shim and fuel section.
With this poisoning, the reactor was critical with shim fuel sections in all
fixed control rod positions, and No. 7 rod withdrawn 12 inches.

Using the relationship

$$k_{excess} = \frac{\Sigma_{poison}}{\Sigma_{poison} + \Sigma_{core}},$$

III-1

where

k_{excess} = the excess reactivity controlled by the gray rods,

Σ_{poison} = the macroscopic absorption cross section of the
distributed poison,

Σ_{core} = the macroscopic absorption cross section of the
homogenized core (excluding experimental holes),

the controlled excess reactivity at start-up was determined to be 11.2% δk/k; the worth of the unused portion of Rod No. 7 was 0.6% giving a total value of 11.8% δk/k.

c. Neutron Flux Distributions (D. L. Parry and J. W. Henscheid)

Neutron flux measurements were made in both the 54 and 51 element cores so that heat generation distributions could be calculated. Since it was decided early in the program that the 54 element core would be the loading configuration in the ETR, more extensive measurements were made on this core than on the other. The horizontal midplane flux was measured in each fuel element as presented in Fig. III-1. The measurements which were made in the 51 element core are presented in Fig. III-2. The operating power level during these flux measurements was calculated from the average fission rate. The accuracy of this calculation is questionable because in the MTR and ETR some difficulty has been experienced in correlating the results from this type calculation with calculations using ΔT and water flow.

When making a full core flux map, it is not possible to remove all foils from the reactor immediately. Since the ETRC is a beryllium reflected reactor, the gold activation by the (γ,n) contribution from the beryllium after the reactor is scrammed gives an error in flux measurement. To determine the importance of this error, gold foils were placed in the reactor immediately after it was scrammed. It was found that this activation, even in those positions adjacent to the beryllium, was less than 0.1% of the activation during the operating period of 22 minutes. In Fig. III-3 the power reduction as measured by the level chambers for the same experimental conditions is presented.

3. ETR Weighting Functions for Fuel and Boron (P. W. Healy)

As discussed previously,[13] predictions of the charge life of various fuel loadings depend upon knowing the weighting function of the effect upon reactivity for fuel and poison at each fuel element position in the core. Preliminary analysis of experimental data[13] from 14 core positions with two control rod patterns indicates that large variations occur in both functions for the different patterns. In one position (I-5) the boron weighting function was 4 times larger in the second run than in the first, and the fuel weighting function was 3 times as large.

In order to avoid making a comprehensive measurement of weighting functions for each loading and rod pattern, a program is being investigated of calculating the adjoints of the fast and slow neutron fluxes as proposed in IDO-16379.[14] These adjoints, in combination with the measured flux, are hoped to yield the weighting functions without their direct measurement. Calculations of the adjoints show that they vary considerably. The minimum variation was 11% for boron and 4% for fuel. Calculations are now being made to determine how great an effect these variations will have on charge life.

(13) P. W. Healy and J. W. Henscheid, Quarterly Progress Report for MTR-ETR Technical Branches, Fourth Quarter - 1957, IDO-16436, 17.

(14) H. L. McMurry and P. W. Healy, Calculation of ETR Charge Life Using ETR Critical Facility Data, IDO-16379, (1957).
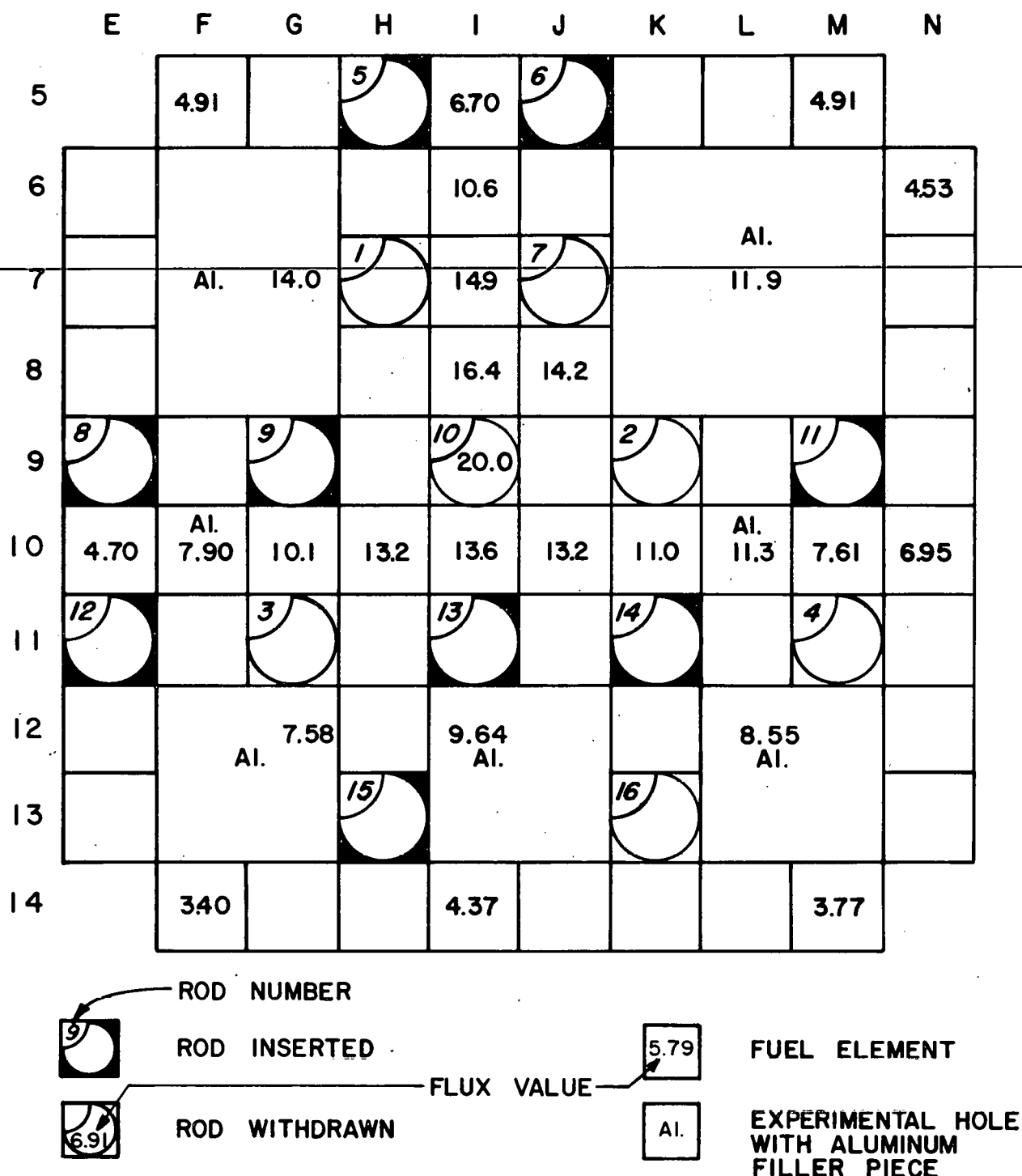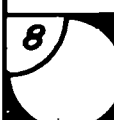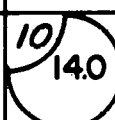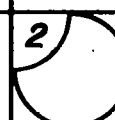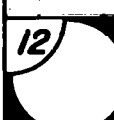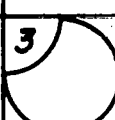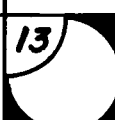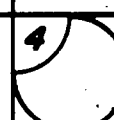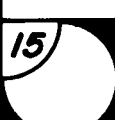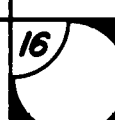
Fig. III-1. The 51 element loading arrangement for the ETRC with horizontal midplane thermal flux values in units of 10^8 neuts/cm^2 sec. The operating power was 320 watts and the No. 7 rod was at 22.5 inches.

Fig. III-2. The 54 element loading arrangement for the ETRC with horizontal midplane thermal flux values in units of 10^8 neuts/cm^2 sec. The operating power was 390 watts and the No. 7 rod was at 26.5 inches.
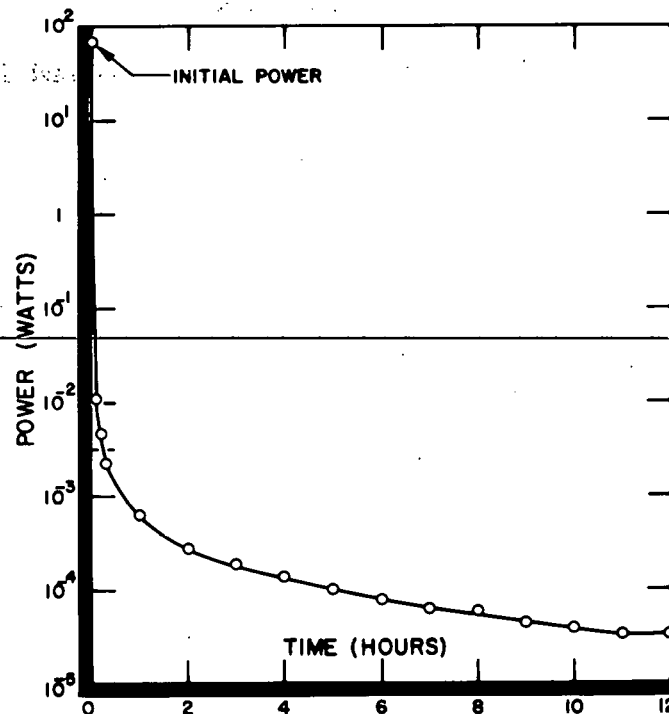
Fig. III-3. The ETRC power as a function of time after scram as measured
by the level meters. The reactor was scrammed after operating at the
initial power for 22 minutes.

4. ETRC Control System Modifications (F. A. Meichle)

It is planned to add a second driven grey rod in position H-13 and
to relocate some of the instruments in the reactor console. This will allow
more flexibility in the operation of the ETRC. The design, drawings, and
wiring schedules are completed for these modifications.

B. ETR Developments

1. Magnet Design and Transient Power Studies (K. V. Moore, H. W. Davis,
S. R. Gossmann, W. J. Byron)

In connection with the redesign of the ETR clutch magnets to obtain
sufficient holding power, assistance was requested by and given to Operations
Engineering Branch in the electrical design of the magnet itself and in
calculating the transient power overshoots produced in part by the measured
magnet release times. Design assistance involved calculation of pole face
areas, flux and flux paths, core material, and shapes to give low release
times.

Transient power overshoots were calculated by ignoring delayed neutrons and by accounting for all delayed neutrons.

In the first case, taking the kinetics equations and ignoring all delayed neutrons,

$$n(t) = n_o e^{Rt^2/2\ell}$$
III-2

where

$n(t)$ = power level, watts

n_o = power level at $t = 0$, watts

R = reactivity added, $\delta k/sec$

ℓ = prompt generation time, sec

t = withdrawal time, sec.

When $n(t) = n_1$ a signal is generated to drop the rods. Because of delays in the system a time delay, τ, is experienced, mostly through the magnet release time, and the reactor power rises to n_2, the time at which the rods begin to fall to shut the reactor down. The power continues to rise to a maximum and then decreases rapidly. The behavior of the reactor with no delayed neutrons is described as

$$n(t > t_2) = n_1 \ e^{(k_o t'/\ell - agt'^3R'/6\ell)}$$
III-3

where

k_o = maximum reactivity in the core at t_2

t' = time after t_2, sec

ℓ = prompt generation time, sec

ag = effective rod acceleration (function of primary flow), cm/sec^2

R' = rod calibration, $\delta k/cm$

n_1 = power level at which time the rods began to fall, watts.

In the second case, with the delayed neutrons accounted for, the kinetics equations.

$$\frac{dn}{dt} = \left[\frac{k_{eff} (1-\beta) - 1}{\ell} \right] n - \sum_{i=1}^{6} \lambda_i \ c_i$$
III-4

$$\frac{dC_i}{dt} = \frac{k_{eff} \ \beta_i \ n}{\ell} + \lambda_i \ c_i$$
III-5

$$\frac{dk_{eff}}{dt} = R \qquad\qquad \text{III-6}$$

where

k_{eff} = effective multiplication factor

β = total fraction of delayed neutrons

C_i = concentration of delayed neutrons in i^{th} group

λ_i = decay constant of the ith group of delayed neutrons

β_i = fraction of delayed neutrons in the ith group

were solved simultaneously by an IBM-650 computer sub-routine. The conditions were changed as in the first case so that after t_2, Eq. III-6 becomes

$$\frac{d^2 k_{eff}}{dt^2} = - ag. \qquad\qquad \text{III-7}$$

A hypothetical case was evaluated by both methods. It was assumed that the ETR control rods were being withdrawn at full speed as the power passed through 5.25 Mw (3% of normal operating power). Conditions were specified in each case that k_{eff} = 1 at n_o = 5.25 Mw. The scram level, N_1, is assumed to be 263 Mw (1.5 normal operating power). The power level as a function of time and the total integrated energy released were calculated. Delay times for accelerations associated with no flow and full flow were accounted for and included in the computations. The cases considered are summarized in Table III-3, and the data are shown graphically in Fig. III-4. These data have been given to Operations Engineering for their calculations of heat flux and fuel element temperatures.

TABLE III-3

Summary of Cases and Pertinent Data

	Acceleration (g)	Maximum Power, n_m (Mw)	Total Integrated Energy (Mw sec)	
Case 1	3	602	54	(no delayed neutrons)
Case 1 (a)	3	317	125	(delayed neutrons)
Case 2	0.7	992	104	(no delayed neturons)
Case 2 (a)	0.7	347	142	(delayed neutrons)

(3g is estimated for full flow, 0.7 g is measured in ETRC for zero flow)

LEGEND

I BLACK + 12 GRAY RODS MOVED AT HIGH SPEED

n_o = 5.25 Mw n_1 = 263 Mw

POWER (MEGAWATTS)

TIME (SECONDS)

	1	**2**	**1a**	**2a**
	n_m = 602 Mw	n_m = 992 Mw	(WITH DELAYED NEUTRONS)	
	E = 54 Mw sec	E = 104 Mw sec	n_m = 317 Mw	n_m = 347 Mw
	FULL FLOW	NO FLOW	E = 125 Mw sec	E = 142 Mw sec
			FULL FLOW	NO FLOW
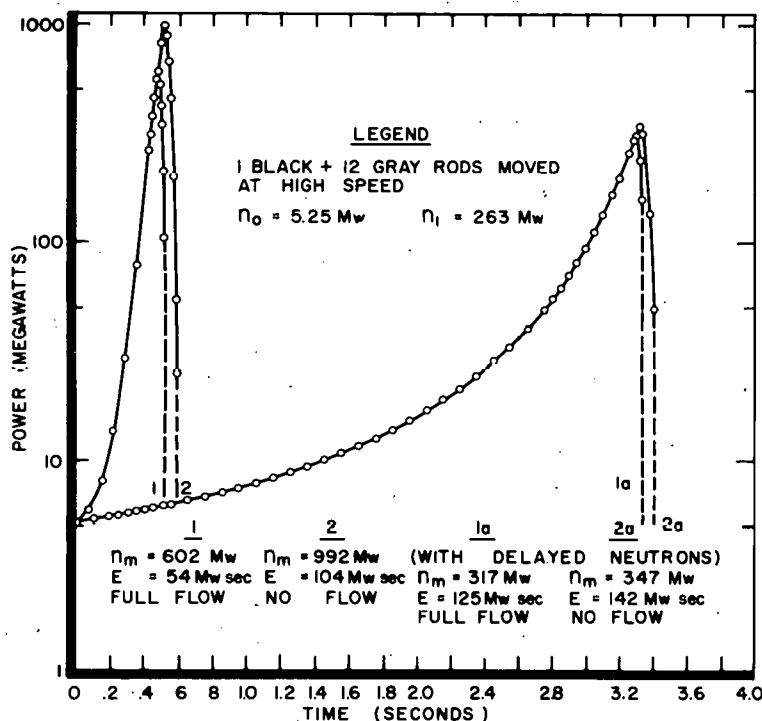
Fig. III-4. Calculated power as a function of time for the ETR assuming full speed withdrawal of the rods. It has been assumed for all cases that k_{eff} = 1 at 5.25 Mw and the scram level is set at 263 Mw. The various cases are summarized in Table III-3.

2. Modifications of the Regulating Rod Controller (F. L. Petree)

Early in 1958, the ETR Operations Branch requested a study of the ETR servo system to determine changes to correct the following operational problems:

(1) Due to insufficient sensitivity it was necessary to place the servo ion chamber in a valuable irradiation space in order to obtain sufficient current for the servo amplifier.

(2) When the regulating rod was stalled in the fully withdrawn limit position a very large error signal was necessary to start insertion. On release the large error signal frequently inserted the rod rapidly enough to reach the lower limit switch causing automatic shim rod insertion.

(3) When approaching either mechanical limit at high speed, the regulating rod struck the limits causing mechanical damage to the rod.

The proposed solutions to these problems are the replacement of the pre-amplifier with a new unit with more gain and a modification of the servo amplifier. Operational tests indicate that the changes will correct the problems.

Fig. III-5 shows a circuit diagram of the proposed new preamplifier. The gain is adjustable from 10 to 100 (in contrast to 1 for the original preamplifier) to allow optimum adjustment for chamber sensitivity and position in the reactor. The reference voltage is adjustable from - 0.5 to - 5 volts whereas that for the previous preamplifier was fixed at 50 volts. The input grid current will be less than 10^{-12} amperes.

Table III-4 shows the range of input currents over which the proposed preamplifier can be adjusted as well as the actual operating conditions that are obtained in the ETR servo chamber.

TABLE III-4

Possible Adjustments of the Proposed Preamplifier

Reference Voltage (v)	Reactor Power	Chamber Current (μamp)	MOR Resistance (meg)	Pre-Amp Gain	Time Constant (msec)	Calculated Output Noise (mv)
-0.5	N_ℓ	0.01	50	100	100	63
-0.5	N_f	1.0	0.5	100	16	30
-0.63	N_ℓ	0.012	50	80	100	58
-0.63	N_f	1.2	0.5	80	12	30
-5.0	N_ℓ	0.1	50	10	100	20
-5.0	N_f	10	0.5	10	1.6	30

N_f = normal operating power
N_ℓ = 1% normal operating power
MOR = motor-operated rheostat

A problem of primary concern in such a high gain dc amplifier is that of drift. In Table III-5 a drift record is shown for a preliminary model of the new preamplifier. Similar drift in an operational preamplifier on the ETR would result in power drifts of approximately 7%. Variations of this type are expected to be reduced by a careful "warm-up" of the operational amplifier and by changing the method of balancing.

It was also found that considerable noise (100 to 200 mv) appeared at the output from the test preamplifier. This noise is caused by statistical fluctuations in chamber current and has the same effect as hum pickup; it causes "grid leak bias" to develop in the output tubes of the servo amplifier so that the output meters deflect downward.

FIG. III-5

SERVO PREAMPLIFIER SCHEMATIC DIAGRAM

1. USE 2 W. A.B RESISTORS WHERE NOT DESIGNATED
2. USE A-B CARBON POTENTIOMETERS
3. V1, V2, V3, & V4 TYPE 5965, 5814, 12AU7A OR 12AJ7

TABLE III-5

Record of Drift in Test Preamplifier

Time (hr)	Equivalent Input (mv)
0	0
1	15 (not a max)
20	20 max
50	10 min
90	30 max
124	23 min
142	40 max

This problem is solved fairly well at high powers by inserting a low-pass filter in the preamplifier. The filter consists of a 0.04 µf capacitor from grid to grid of V3 in Fig. III-5. The feedback in the preamplifier changes the time lag characteristic of this filter when the gain is adjusted; it is found that this change should theoretically compensate exactly for the changes in noise and preamplifier gain so that the noise in the preamplifier output will be 30 mv at operating power (N_p) for any set-point adjustment. In the ETR, the input circuit, which includes the motor-operated rheostat (MOR) and input capacitance, forms another filter whose effect is negligible at N_p; at the lower limit of servo control (1% of normal power or N_ℓ), however, the MOR resistance is so high that its filtering action predominates over the effect of the 0.04 µf capacitor. In Table III-4 are shown the theoretical values of the output noise for different conditions of set-point and MOR resistance.

The disadvantage of using low-pass filters is that they introduce a time lag which tends to cause unstable operation. From Table III-5 it is seen that this effect is most pronounced at low power (N_ℓ). This preamplifier effects a "best" compromise between excessive noise and excessive time lag.

Two modifications are proposed for the servo amplifier as shown in Fig. III-6. The application of tachometer feedback at the input when the regulating rod comes to either limit provides dynamic braking. The insertion of relatively large resistors in the cathodes of the output amplifiers, when the rod comes to either limit, drastically reduces the field current of the amplidyne; and thus reduces the stall torque.

In the modification in the output circuit, when K2 or K3 de-energizes as the regulating rod approaches the inner or outer limit, respectively,

resistors are inserted in the cathode circuit of the output tubes. These limit the currents in V14 and V15 to values that are just sufficient to move the rod. Since a smaller error signal is necessary from a cocked position, the rod inserts smoothly out of the limit.

The other modification, that of the input circuit, slows the rod electrically as it approaches a mechanical stop. K3 and K2 contacts, each in series with a germanium diode, are in parallel with R8, the adjustable damping resistor. Now, if the rod approaches the outer limit, K2 de-energizes and connects a diode across R8. The polarity of this diode is such that it shorts R8 as the rod drives against the limit. This applies full tachometer feedback to the amplifier of such polarity to brake the rod abruptly so that it gently strikes the outer mechanical stop. This braking action does not operate when the rod withdraws from the limit because the polarity reverses and the diode cuts off.

FIG. III-6
ETR SERVO AMPLIFIER SCHEMATIC DIAGRAM

NOTES —
1. ALL RESISTORS 1W, ±10% EXCEPT AS NOTED.
2. ALL CAPACITORS BELOW 1μf ARE MICA.
3. MOUNT RESISTORS NOTED DIRECTLY ON TUBE SOCKET.
4. ALL RELAYS SHOWN DE-ENERGIZED.
5. IT IS IMPERATIVE THAT POLARITY OF CONNECTIONS BE OBSERVED.
6. THESE RESISTORS TO BE SELECTED FOR PROPER OPERATION WITH AVAILABLE 1.5 MEG. RESISTORS.
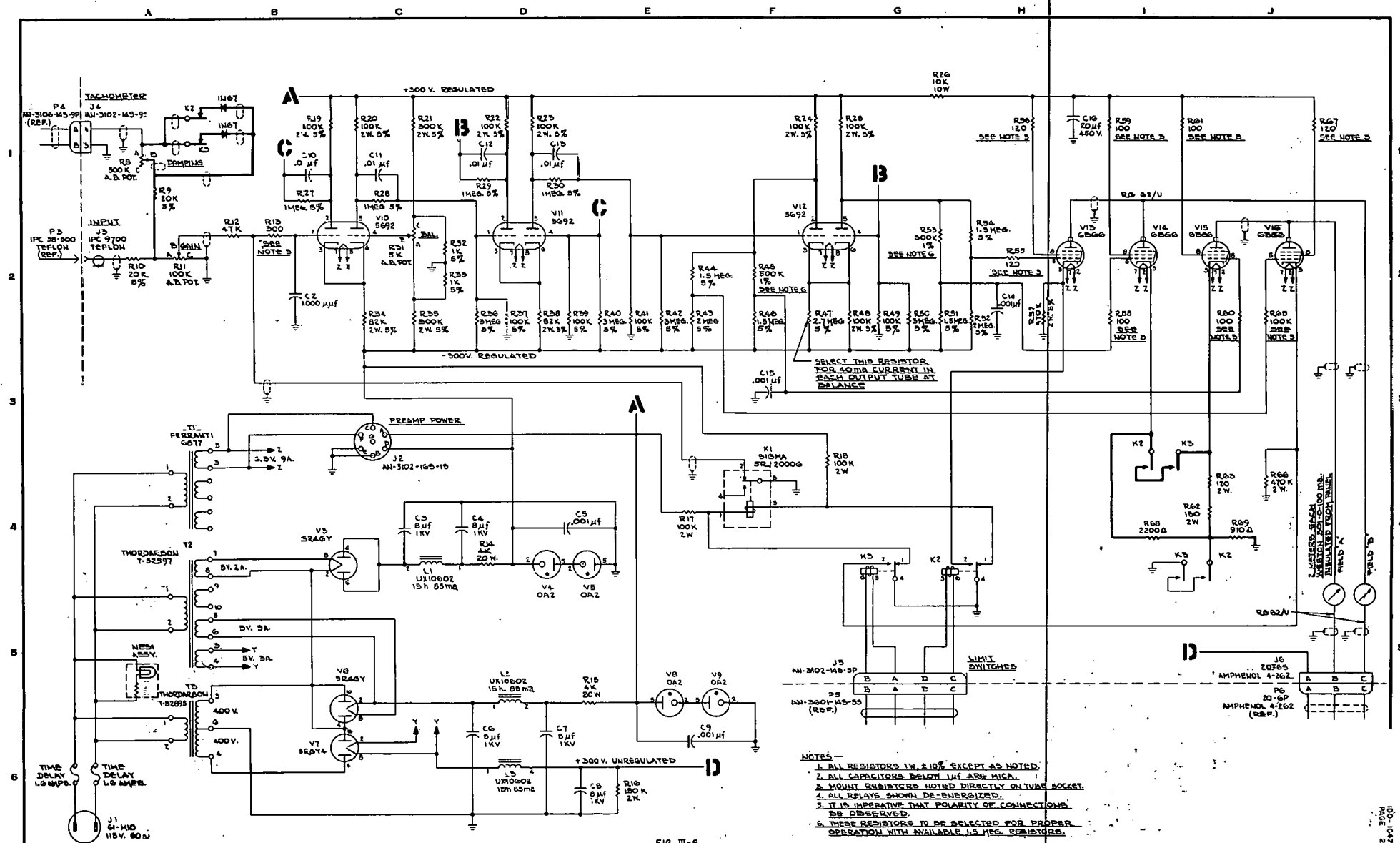
IV. REACTOR PHYSICS AND ENGINEERING

A. Transfer Function Analysis of Heat Exchangers (S. R. Gossmann)

The dynamic behavior of a heat exchanger is pertinent to the problem of determining analytically the transient operation of a reactor such as the ETR. The transfer functions of the lumped and space dependent heat exchanger models are to be compared to see which fits the actual case better. The transient effects of the heat exchanger affect the reactor power through the temperature coefficient of reactivity. The usual approach taken by most authors[15,16] in describing the transient characteristics of heat exchangers is to assume a lumped system, i.e., a system in which temperature variations are space independent. One result of this assumption is to concentrate the heat transfer at a point; thus the time taken for the fluid to pass through the heat exchanger is ignored. This result may or may not seriously affect the dynamic behavior of a reactor as predicted by the solution of the differential equations representing the reactor core and the heat exchanger. In order to determine whether the representation as a lumped system is sufficiently descriptive of a reactor with heat exchanger, transfer functions for space dependent heat exchangers have been derived. The derivation of the equations for a space dependent heat exchanger is based on the work done by Dr. Yasundo Takahashi of the University of Tokyo.[17]

Let the heat exchanger be represented schematically as in Fig. IV-1. The differential equations for the heat transfer through the heat exchanger are

$$\frac{\partial \theta_1}{\partial \tau} + \frac{\partial \theta_1}{\partial y} = a'_1(\Phi_h - \theta_1) \qquad \text{IV-1}$$

$$\frac{\partial \Phi_h}{\partial \tau} = b_{h_1}(\theta_1 - \Phi_h) + b_{h_2}(\theta_2 - \Phi_h) \qquad \text{IV-2}$$

$$r\frac{\partial \theta_2}{\partial \tau} \pm \frac{\partial \theta_2}{\partial y} = a'_2(\Phi_h - \theta_2) + a'_s(\Phi_s - \theta_2) \qquad \text{IV-3}$$

$$\frac{\partial \Phi_s}{\partial \tau} = b_s(\theta_2 - \Phi_s) \qquad \text{IV-4}$$

* (+) for parallel flow; (-) for counter flow.

(15) M. A. Schultz, Control of Nuclear Reactors and Power Plants, New York, McGraw-Hill, (1955).

(16) R. L. Murray, Nuclear Reactor Physics, New Jersey, Prentice-Hall, (1957).

(17) Yasundo Takahashi, Transfer Function Analysis of Heat Exchange Processes in Automatic and Manual Control, 235-48, New York, Academic Press, (1952).
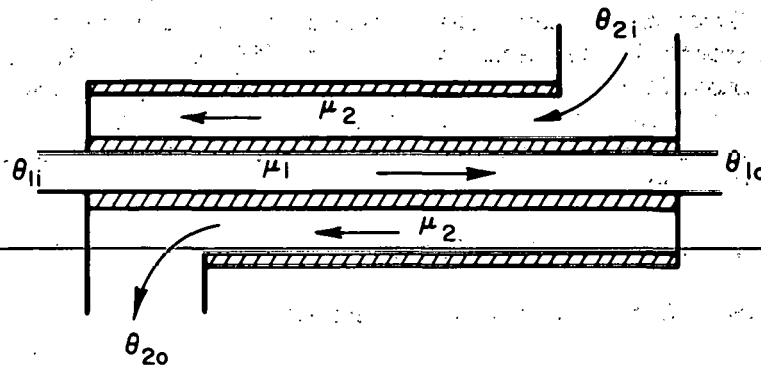
μ_1 = PRIMARY FLOW RATE $\qquad$ θ_{1o} = PRIMARY OUTLET TEMPERATURE

μ_2 = SECONDARY FLOW RATE $\qquad$ θ_{2i} = SECONDARY INLET TEMPERATURE

θ_{1i} = PRIMARY INLET TEMPERATURE $\qquad$ θ_{2o} = SECONDARY OUTLET TEMPERATURE

Fig. IV-1. A schematic representation of a heat exchanger.

The transfer function of interest in the ETR analysis is

$$\frac{\theta_{1o}}{\theta_{1i}}(j\Omega) = \frac{(-p_1+f_2)e^{p_1}-(-p_2+f_2)e^{p_2}}{p_1-p_2} + \frac{g_1(e^{p_2}-e^{p_1})}{p_1-p_2}\frac{\theta_{2o}}{\theta_{1i}}(j\Omega) \text{ or} \qquad \text{IV-5}$$

$$\frac{\theta_{1o}}{\theta_{1i}}(j\Omega) = \frac{(-p_1+f_2)e^{p_1}-(-p_2+f_2)e^{p_2}}{p_1-p_2} + \frac{g_1g_2(e^{p_2}-e^{p_1})(1-e^{p_1-p_2})}{(p_1-p_2)\left[-(p_1-p_2e^{p_1-p_2})+f_2(1-e^{p_1-p_2})\right]} \qquad \text{IV-6}$$

(Definitions of the symbols for the above equations follow as a separate list.)

Since no evaluation has yet been performed with this transfer function, no direct comparison exists between the space dependent and the lumped representation of the heat exchanger. The necessary calculations will soon be performed.

The transfer function $\frac{\theta_{1_o}}{\theta_{1_i}}(j\Omega)$ was derived from the differential equations given above.

One serious limitation of this transfer function is that both primary and secondary flow rates have been assumed to be constant. The case of particular interest in the analysis of the ETR is that in which the secondary flow rate is allowed to vary with time independently of the temperatures. The deriviation of the transfer function expressing this condition requires further modification and linearization of the differential equations. This work is presently being performed.

Definition of symbols and functions:

1 = primary side of the heat exchanger

2 = secondary side of the heat exchanger

h = inner wall

i = inlet

o = outlet

s = outer wall

θ_1, θ_2 = temperature of primary and secondary fluid, respectively

Φ_h = temperature of inner metal wall

Φ_s = temperature of outer metal wall

μ = flow rate

t = time

ℓ = total passage length

$L = \ell/\mu$ transportation lag, $L_1 = \ell/\mu_1$, $L_2 = \ell/\mu_2$

Y = running length along primary side

$y = Y/\ell$

$\tau = t/L_1$

α = surface coefficient of heat transfer

U = perimeter of heat exchange surface

$F = U\ell$

W = heat capacity of fluid per unit length

$q = W\mu$; $q_1 = W_1 \mu_1$; $q_2 = W_2 \mu_2$

$$a'_1 = \alpha_1 F_1/q_1$$

$$a'_2 = \alpha_2 F_2/q_2$$

$$a'_s = \alpha_s F_s/q_2$$

C_h = distributed solid heat capacity per unit length along the flow

$$b_h : b_{h_1} = \alpha_1 F_1/C_h \mu_1; \quad b_{h_2} = \alpha_2 F_2/C_h \mu_1; \quad b_s = \alpha_s F_s/C_s \mu_1$$

$$r = \mu_1/\mu_2$$

ω = angular frequency

$$\Omega = \omega L_1$$

$$j = \sqrt{-1}$$

$$f_1 = j\Omega + \frac{a'_1(b_{h_2} + j\Omega)}{b_{h_1} + b_{h_2} + j\Omega}$$

$$f_2 = j\Omega(r + z) + \frac{a'_2(b_{h_1} + j\Omega)}{b_{h_1} + b_{h_2} + j\Omega} \quad \text{where } z = \frac{a'_s}{b_s + j\Omega}$$

$$g_1 = \frac{a'_1 b_{h_2}}{b_{h_1} + b_{h_2} + j\Omega}$$

$$g_2 = \frac{a'_2 b_{h_1}}{b_{h_1} + b_{h_2} + j\Omega}$$

$$p_1 = 1/2 \left[-(f_1 - f_2) + \sqrt{(f_1 + f_2)^2 - 4 g_1 g_2} \right]$$

$$p_2 = -p_1 - (f_1 - f_2)$$

B. <u>Heat Transfer Experimental Program</u> (M. L. Griebenow)

Heat transfer experiments are aimed at obtaining data in the nucleate boiling region, at burnout, and in the film boiling region, to provide data for operating reactors under conditions of nucleate boiling. Exploratory in-pile boiling heat transfer experiments were conducted in the MTR in 1956. Out-of-pile tests, followed by a continuation of the in-pile experiments, are now proposed.

The status of the heat transfer experimental program at the MTR was reviewed with the Heat Transfer Subcommittee of the Phillips Reactor Safeguard Committee on February 27, 1958. Program planning has been continued and some exploratory out-of-pile testing was started. A brief discussion of some of the experimental areas under consideration was

presented in the previous MTR-ETR quarterly progress report.[18] The
Operations Evaluations Group is designing a series of experiments to determine
the significant independent variables with a minimum of experimental effort.

Exploratory experiments consisting of observing the reaction of droplets
of water in contact with heated aluminum have been performed. These experi-
ments are intended to show the temperature range in which burnout occurs
under conditions of natural convection and to yield some film boiling data.

A bi-metallic heat transfer test section is being assembled for forced
convection heat transfer experiments in the nucleate boiling and film boiling
regions. This unit consists of a 0.250" thick aluminum muff 36" long
metallurgically bonded to a 0.375" stainless steel tube. The aluminum muff
will be incased in an alundum furnace core wound with a 220-volt 3-phase
nichrome resistance coil. The entire test section will be adequately insulated.
Eight thermocouples placed in the aluminum will be used to determine the tube
surface temperature. The inlet and outlet coolant temperatures will be
measured by conventional thermocouples and the average heat transfer rate will
be determined.

C. Metal-Water Reaction Program (W. F. Zelezny, D. E. Williams)

The objective of the metal-water experimental program is the development
of methods of measurement of the reaction rates between water and metals at
temperature levels both below and above the melting points of the metals.
The fundamental data thus obtained will aid in understanding the variables
of the metal-water reaction and in predicting the potential hazard involved
in water-cooled nuclear reactors.

The first phase of the out-of-pile experiments was initiated to determine
isothermal reaction rates between water and aluminum at temperatures above
the melting point. The apparatus used for these tests is illustrated in
Fig. IV-2 and consists of a reaction vessel to permit dropwise addition of
water to molten aluminum.

The vessel is flushed with a stream of argon gas before and during the
melting of the aluminum sample. When the aluminum sample has reached the
desired operating temperature the system is sealed (except for the safety
valve arrangement) and the addition of water droplets to the molten aluminum
is begun. The argon within the system is circulated at a rate of about 1 1/2
liters per minute throughout the melting and reaction periods. A cold trap
cooled with dry ice is provided to prevent the accumulation of excess moisture
in the system.

Samples of the gas within the apparatus are withdrawn at the beginning
and at the end of a run and analyzed by means of the mass spectrograph to
determine the precentage of H_2 gas which has accumulated during the run.
The H_2 gives a measure of the extent of the reaction which has taken place
between the aluminum and the water. When a circulating pump of higher
capacity is obtained to keep the hydrogen gas uniformly mixed with the argon
at all times, it will be possible to sample the gas at intervals throughout
the run. In this manner changes in the rate of the reaction with time may
be observed.

(18) M. L. Griebenow, J. R. McGeachin, and E. H. Porter, Quarterly Progress
Report for MTR-ETR Technical Branches, Fourth Quarter - 1957, IDO-16436,
45-59.
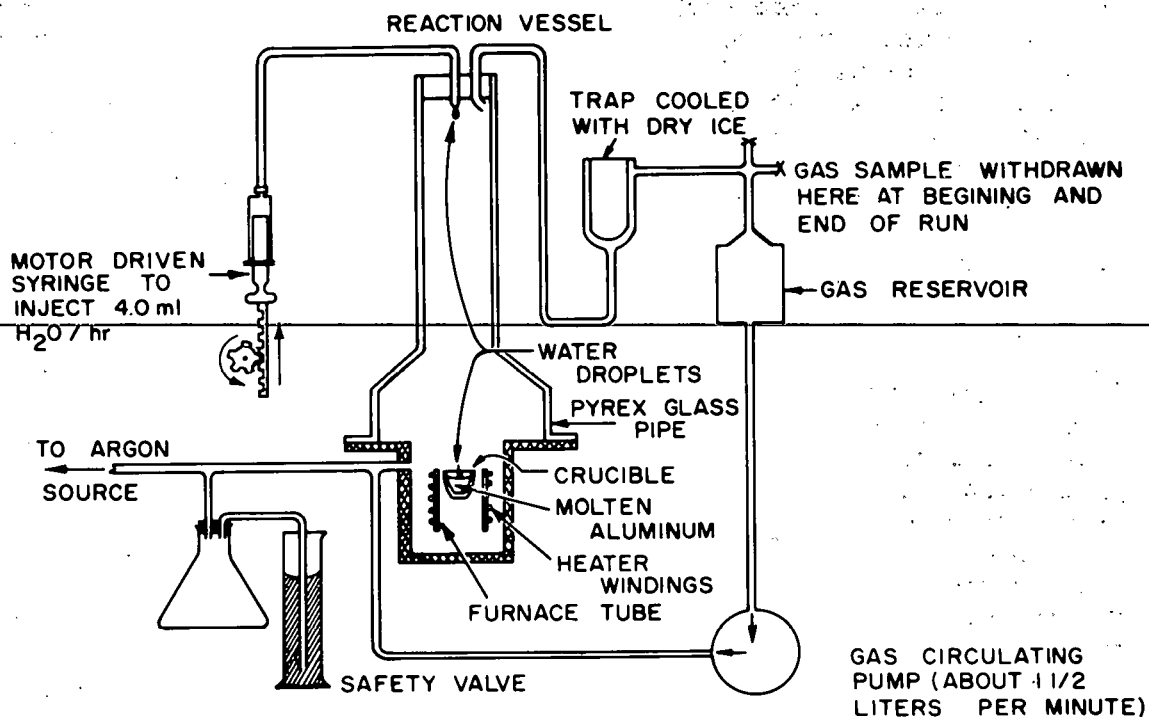
Fig. IV-2. A schematic diagram of the metal-water reaction apparatus.

While more work is necessary to establish the conditions of maximum reproducibility, the results shown in Table IV-1 are typical of those obtained thus far.

TABLE IV-1

Typical Metal-Water Reaction Test Results

Quantity	Numerical Value
Length of run	1 1/2 hours
Sample	30 g of 1100 aluminum
Temperature of aluminum	1400° F
Water added	6.0 ml in 1.5 hours
Water reacted	3.8%
Aluminum reacted	0.73%

The behavior of the water droplets on the molten aluminum surface (or more properly the oxide surface on the molten metals) depends in a very sensitive manner on a number of still undefined variables, such as the composition of the alloy. When water droplets were added to molten 6061 aluminum they remained quietly in place for 30 to 60 seconds until evaporation was complete. With 1100 aluminum, more variable and irreproducible behavior was observed, the drops in some cases remaining only 1 to 2 seconds, and in other cases up to 20 seconds before evaporation was complete.

D. Thorium Program (R. G. Nisle)

Calculations of production of U^{233} from Th^{232} by cyclic and continuous irradiation have been continued and extended. The 16-5 (16 days irradiation, 5 days decay) and 16-26 day cycles calculations have been extended to 10 cycles. Although calculations indicated no significant difference after 5 cycles of irradiation, after 10 cycles it was found that the net U^{233} production was slightly less for cycled (16-26) than for continuous (16-5) irradiation for both cycle times. Table IV-2, which summarizes the results on a 10 cycle irradiation using the 16-26 day cycle, illustrates the fact that whatever U^{233} is lost by cycling has been fissioned or is potentially fissionable as U^{235}. Hence, continuous irradiation is preferable if the only interest is in U^{233} production. On the other hand, no loss of net energy results from cyclic operation of a power-breeder reactor.

TABLE IV-2

Summary of Results of Calculations on Cycled vs Continuous Irradiation

Cycle = 16 days irradiation - 26 days decay, $\emptyset = 10^{14}$ neuts/cm^2 sec, initial $Th^{232} = 3 \times 10^{22}$ atoms. Net nvt the same for both cycled and continuous irradiations.

Element	Nuclei After 10 Cycles Irradiation	Nuclei After Continuous Irradiation
Pa^{233}	3.9143×10^{19}	7.4367×10^{19}
U^{233}	1.9023×10^{20}	1.7026×10^{20}
Sum Pa^{233}, U^{233}	2.2937×10^{20} (1)	2.4462×10^{20} (2)
U^{234}	1.2806×10^{19}	1.4932×10^{19}
U^{235}	3.7138×10^{17}	4.3017×10^{17}
U^{233} fissioned	7.4908×10^{19}	5.7436×10^{19}
U^{235} fissioned	1.0013×10^{17}	1.1495×10^{17}
Sum U^{234}, U^{235}, and fissioned nuclei	8.8186×10^{19} (3)	7.2913×10^{19} (4)

Difference: Item (2) - Item (1) = 1.525×10^{19} atoms
Difference: Item (3) - Item (4) = 1.527×10^{19} atoms
Fissioned plus fissionable nuclei = 3.0475×10^{20} atoms (cycled)
Fissioned plus fissionable nuclei = 3.0260×10^{20} atoms (continuous)

Measurements of the build up of U^{233} from decay of Pa^{233} in irradiation slugs are continuing. About 4 half-lives have elapsed since these slugs were removed from the MTR. Hence, the U^{233} content should be approaching its equilibrium value. The estimated increase in U^{233} content since removal from the MTR is 0.2 to 0.3 grams in about 900 grams of thorium. Some of the reactivity measurements on these slugs have been rather erratic, hence, these results should be considered tentative until confirming measurements have been made.

E. RMF Control Element Modifications (E. Fast, W. J. Byron)

A revised shim rod and an auxiliary fine control regulating rod have been installed in the RMF. The new design allows support of the entire assembly above the water level. The increased support rigidity, together with a more rigidly constructed neutron absorber element, should improve the reproducibility of measurements. The auxiliary regulating rod consists of a fine cadmium wire element on a stainless steel wire mounted with its structural tubing in RMF position 4-7 about 1.6 inches from the active lattice. The poison wire can move a vertical distance of 9 inches for a total reactivity worth of approximately 5×10^{-5} $\delta k/k$. Measurements can be read directly to 1×10^{-7} $\delta k/k$. This rod can be used in servo operation of the reactor for measurement of samples having small effect on the reactivity.

F. Fuel Element Development Program (W. C. Francis)

The object of the fuel element development program is to perform design studies, carry out hydraulic, metallurgical, and irradiation tests on fuel compositions, develop assembly techniques, and study geometries resulting in improved fuel assemblies and shim rods for reactors. Details of hydraulic tests performed on five fuel elements, static pressure tests performed on two fuel elements, irradiation of sample fuel plates, and progress on a new shim rod design are described in the following sections.

1. Hydraulic Tests (J. R. McGeachin)

The objectives of the hydraulic tests are: (1) The measurement of flow through the fuel element vs pressure drop. (2) The determination of the maximum flow rate obtainable through the fuel section without fuel plate buckling. (3) The correlation of pressure drop across the assemblies with temperature change. (4) The comparison of measured values with calculated values. All of these tests were performed in the single element hydraulic test loop located at the MTR.

a. MTR Production Type Elements

Two MTR production type elements, but with depleted cores, were tested hydraulically to determine flow vs pressure drop and the maximum flow rate at failure. The tests were run at two different temperatures in order to measure the change in coefficient of friction with change in kinematic viscosity. The pressure drop across the end boxes of the elements proved to be independent of the temperature in the range in which the tests were conducted ($80°$ to $120°$ F) and the measured change in pressure drop due to change of temperature agreed with the calculated values. Element No. 1 was run at a maximum bulk velocity of 39.75 ft/sec (fuel section average velocity)

for a short period of time without any evidence of plate buckling. Limitations of the test loop did not permit operating at higher flow rates. The lateral differential pressure across the outside fuel plates of the element was increased until buckling of the outer fuel plate occurred. Because of the high flow rate through the element when failure occurred, the damage propagated throughout the element. The failure was observed by a rapid increase in pressure drop across the element and a rapid decrease of flow through the assembly. The maximum lateral differential pressure across the outside fuel plate was about 14 psi at failure.

Element No. 2 was tested primarily for the pressure drop correlation with respect to temperature. The plotted data showed a 2/3 psi increase in the level of the pressure drop curve between an average velocity of 30.5 ft/sec and 33.5 ft/sec indicating that failure occurred during the test. This slight increase in pressure drop could not be detected during testing. Inspection of the element after testing revealed that one center fuel plate had failed. This fuel plate was cut from the element for examination. The cause of failure was determined to be the lack of brazing of the fuel plate to the side plate for about 8 inches along one side. Fig. IV-3 shows a photograph of the fuel plate showing this unbrazed section and the fuel plate with the cut portion of the side plate pulled away. Center lines marked on the fuel plate indicate the location of the bulge. Fig. IV-4 presents the flow-pressure drop results of tests run on both elements. The overall pressure drop measurements have been corrected to an inlet and exit area of 12.25 square inches (3.5" x 3.5").

b. Tubular Fuel Element

Two depleted tubular fuel elements for out-of-pile hydraulic tests have been received from the vendor as part of the fuel element development program. Sixty-four fuel tubes have been encased in a shell having the contours of an MTR fuel element. The four sides of this shell have plenums (3/4" in diameter) for relief of the lateral differential pressures. By means of these holes and a plexiglass window installed in the hydraulic test holder, visual observation of the fuel tubes during testing is possible. Preliminary hydraulic tests have shown a slight lateral shifting of the tube bundle itself. The average frequency of this shifting is estimated at 1/2 to 1 cycle per second, independent of the flow rate. The determination of the vibration of a single tube is being attempted by ultrasonic techniques. Velocity contours and life tests are also scheduled.

2. Transparent Flow Test Fixture (E. H. Porter)

An experimental variable channel test fixture has been fabricated with transparent side plates. Direct observation of the flow in various sized channels is expected to yield valuable data on velocity distribution. The design of the fixture is similar to that of an existing metal fixture and permits complete interchangeability in the hydraulic loop pumping facilities.

The material chosen for the fixture is a clear plastic with the trade name of "Homalite". In appearance it is like "Lucite" or "Plexiglass", but its surface hardness, abrasion resistance, and tensile strength are superior to those of the more common clear materials.
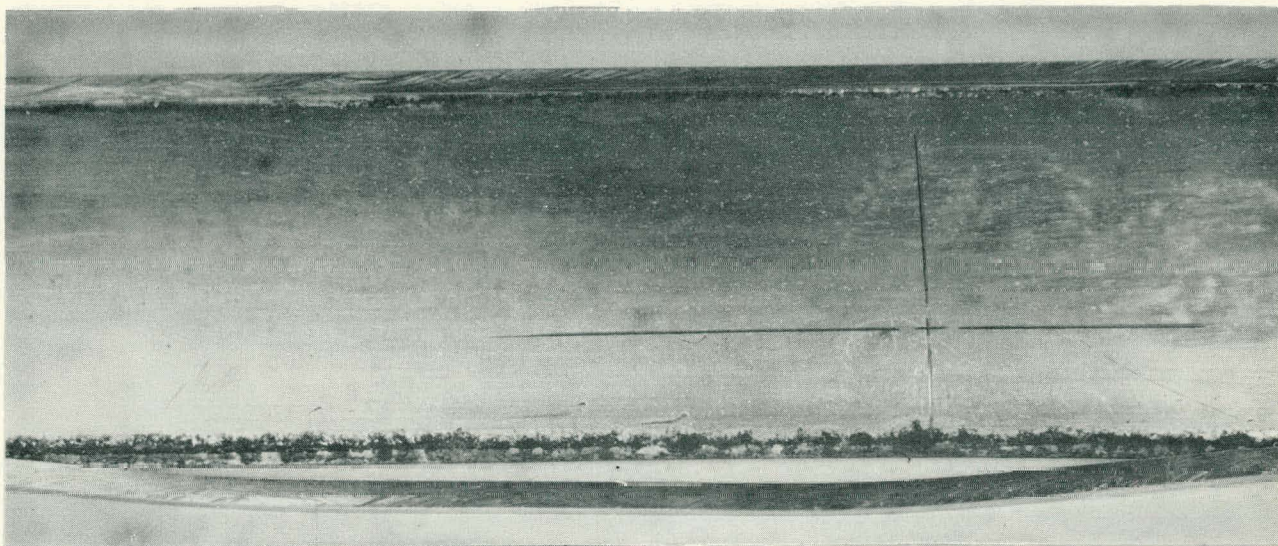
SECTION OF NON-BRAZED SIDE PLATE
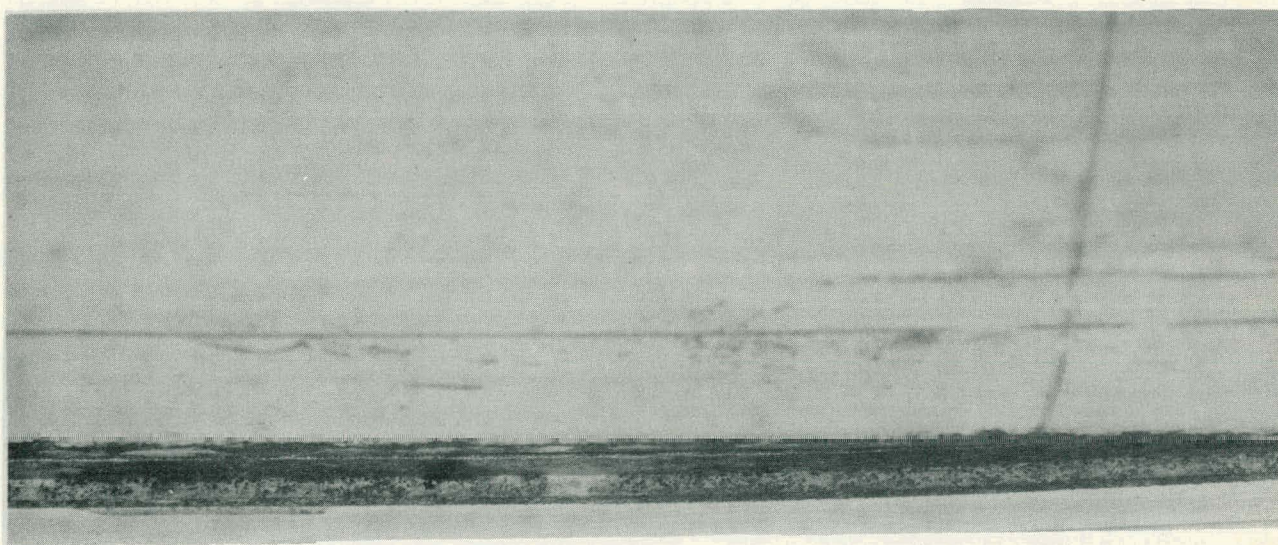
NON-BRAZING ON SIDE PLATE
(CLOSE-UP VIEW)

Fig. IV-3. Section from an MTR production type fuel element showing a damaged fuel plate removed from the fuel section. It shows a lack of brazing for about 8 inches along one side.
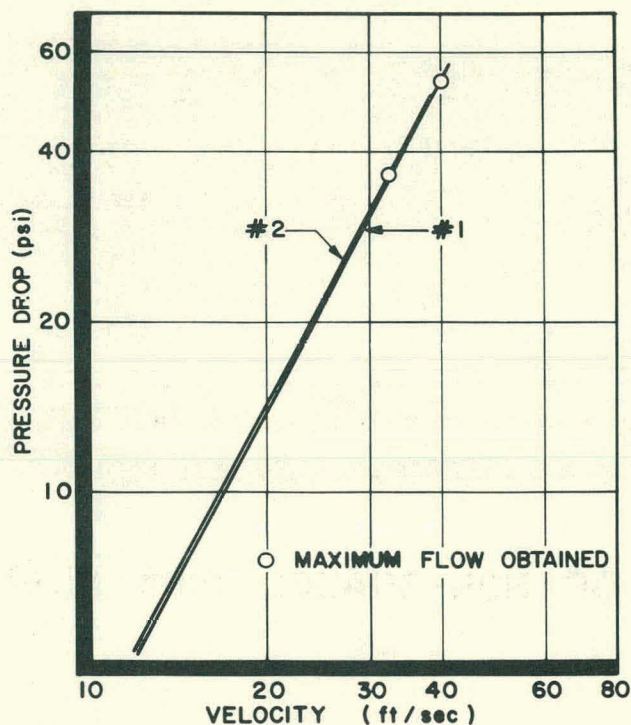
Fig. IV-4. Flow vs pressure drop through an MTR fuel element at an average water temperature of 120° F. The pressure drop across the element has been corrected to an area of 12.25 square inches above and below the element.

3. Static Pressure Tests (J. A. Alexander, D. D. Jeffries)

One of the first production MTR fuel elements fabricated by the current supplier was subjected to static pressure tests. These tests involve the application of air pressure internally to the fuel element while measuring the deflection of the outside plates. By releasing the pressure after each measurement, the onset of a permanent deflection can be determined. The resulting pressure-deflection curve closely paralleled previous MTR fuel element test results up to about 8 psi. Beyond this pressure the deflection was greater than in previous tests. Plate reversal on the element occurred at 19 psi compared to 23 psi for earlier MTR elements. Permanent deflection first occurred at 9 psi compared to a previous average of 11 psi. Although somewhat inferior to earlier elements, the new element did meet the tentative minimum specification for the test.

4. Sample Fuel Plates (J. A. Alexander, E. H. Porter, D. D. Jeffries)

The investigation of the behavior of various fuel compositions, poisons, and claddings under high flux conditions began with the irradiation of 6 batches of sample fuel plates in December 1957. A total of 316 sample

plates representing 19 of the 21 compositions ordered have been received from the vendor. Only two thorium oxide compositions remain to be delivered. One hundred seventy-one of these plates were received during this quarter. Pre-irradiation metallurgical tests have been completed on 12 of the compositions; tests on the remaining 7 compositions are in progress. Post-irradiation metallurgical tests in the MTR hot cell are scheduled to start in June and will duplicate as closely as possible the pre-irradiation tests.

Twelve compositions are currently being irradiated in the L-51 position in the MTR on an alternate cycle basis. The maximum fuel burnup to date is 28%. Two additional reactor cycles are currently scheduled for each of these compositions to give an estimated fuel burnup of 40%.

The irradiation program has revealed no plate damage caused by the radiation. A slight bending of several of the plates was noticed following two of the irradiation cycles and has been attributed to differential lateral pressures. In order to equalize this lateral pressure a new type plate holder has been designed and fabricated. The first loading with the new holders will be for Cycle 103.

Flux values for position L-51, measured with aluminum-cobalt flux wires, have been obtained for the first three cycles (97, 98, and 99). The flux for the succeeding cycles is also being measured. Fuel burnup is being calculated, using the measured flux values for each cycle. Reactivity measurements have been made on one plate of each composition after each cycle. These data have not yet been correlated.

The original "L" piece container for irradiating the sample fuel plates has given considerable trouble in the removing and replacing of the top end box. An improved disconnect mechanism has been designed which appears to overcome many of the objections of the earlier type. A handling tool for the new "L" piece has also been designed. Upon completion of the construction drawings, three "L" pieces and one handling tool will be fabricated.

G. Decay Time Analog Computer Feasibility Study (R. H. Brown)

Because of the analogy between condenser discharge and radioactivity decay rates, it has been considered desirable to investigate the practicality of building a computer to study radioactive build up and decay times. In order to investigate this technique a test computer was built and a simple problem was solved with it. The basic equations for radioactive decay are

$$N(t) = N_o e^{-\lambda t} \qquad\qquad \text{IV-7}$$

$$A(t) = \lambda N(t) \qquad\qquad \text{IV-8}$$

where

N = number of atoms as a function of time

N_o = number of atoms at t = 0.

λ = decay constant, sec

A = activity as a function of time, disintegrations/sec

The analogous electrical equation for the discharge of a condenser through a resistor is

$$E(t) = E_o \, e^{-t/RC} \qquad\qquad \text{IV-9}$$

where

$\quad$ E = voltage as a function of time

$\quad$ E_o = voltage at t = 0

$\quad$ 1/RC = decay constant, sec^{-1}

From Eq. 7 the general equation for a decay chain can be generalized giving the Bateman equation which is

$$\frac{N_n}{P_1} = C_1 e^{-\lambda_1 t} + C_2 e^{-\lambda_2 t} + \ldots + C_n e^{-\lambda_n t} \qquad\qquad \text{IV-10}$$

where

$$C_1 = \frac{\lambda_1 \lambda_2 \ldots \lambda_{n-1}}{(\lambda_2 - \lambda_1)(\lambda_3 - \lambda_1) \ldots (\lambda_n - \lambda_1)} \,,$$

$$C_2 = \frac{\lambda_1 \lambda_2 \ldots \lambda_{n-1}}{(\lambda_1 - \lambda_2)(\lambda_3 - \lambda_2) \ldots (\lambda_n - \lambda_2)}$$

N_n = number of atoms of nth member as a function of time, and

P_1 = atoms of parent substance at t = 0.

The test computer diagram is shown in Fig. IV-5. An analogous curve for N(t) vs t is obtained in terms of N_o by plotting E vs t for any stage as shown in Fig. IV-6. Also, by measuring the current flowing from a condenser, relative activities, A(t), are obtained as shown in Fig. IV-7. When a suitable recorder is used, λ ratios of 10^5 may be computed with an accuracy of $\pm$ 2% for one standard deviation. By assuming 1 msec = 1 day, over 800 years may be represented within the above limits of accuracy. As many as 5 stages may be computed in this manner with branching occurring in each stage.

The graphs in Fig. IV-6 are as recorded and have not been corrected for the fact that the condensers used in the small computer were not equal. The graphs represent $N_n(t, P_1)$ when corrected for condenser size. Fig. IV-7 is a recording of the currents for the same physical setup as Fig. IV-5. This represents the activities of the first two stages normalized to the activity of the first stage.

STAGE #1   STAGE #2   STAGE #3

6.13 MΩ   .977 μ fd   1.52 MΩ   .942 μ fd

45 V. E_1 $\overrightarrow{I_1}$ E_2 $\overrightarrow{I_2}$ E_3

.508 μ fd

$E_{1(t)} = N_{1(t)}$ $E_{2(t)} = N_{2(t)}$ $E_{3(t)} = N_{3(t)}$

$I_{1(t)} = A_{1(t)}$ $I_{2(t)} = A_{2(t)}$

$\lambda_1 = .321 \text{ sec}^{-1}$ $\lambda_2 = .673 \text{ sec}^{-1}$

IN → OUT   D.C. AMPLIFIER   GND

—ᴠᴠᴠ— CIRCUIT FOR BRANCHING CALCULATIONS
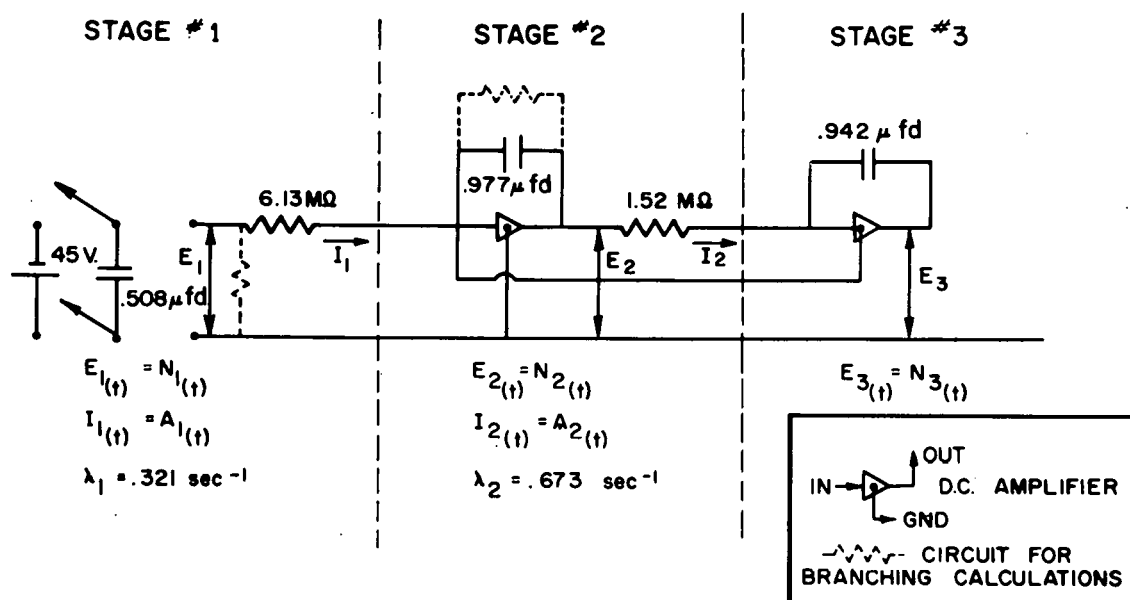
Fig. IV-5. A schematic diagram of the decay time analog computer.
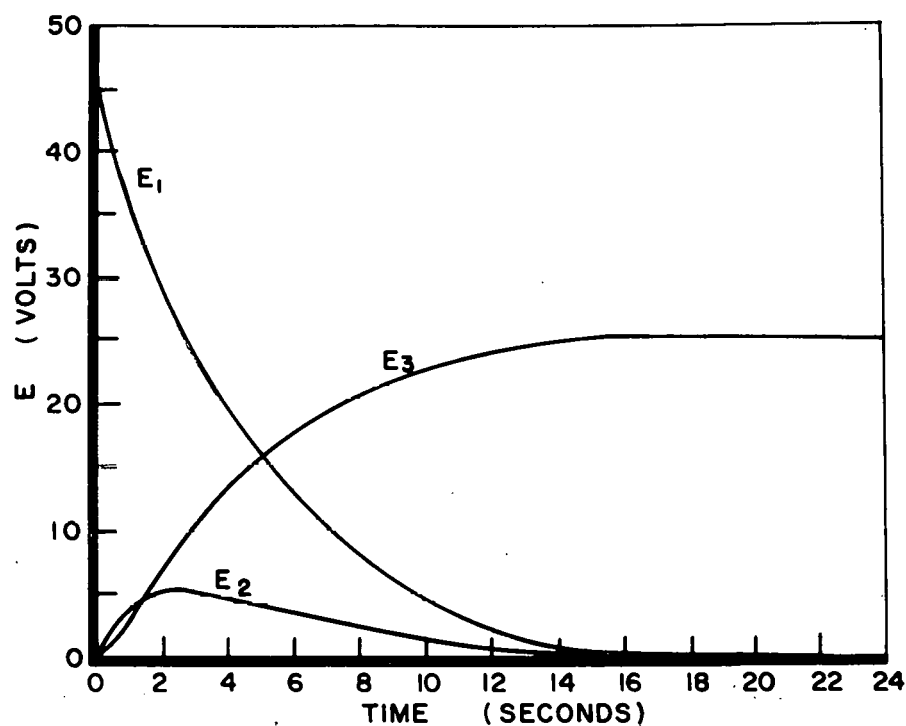
Fig. IV-6. The voltage-time response of the circuit in Fig. IV-5 which is analogous to the number of atoms of a decay chain.
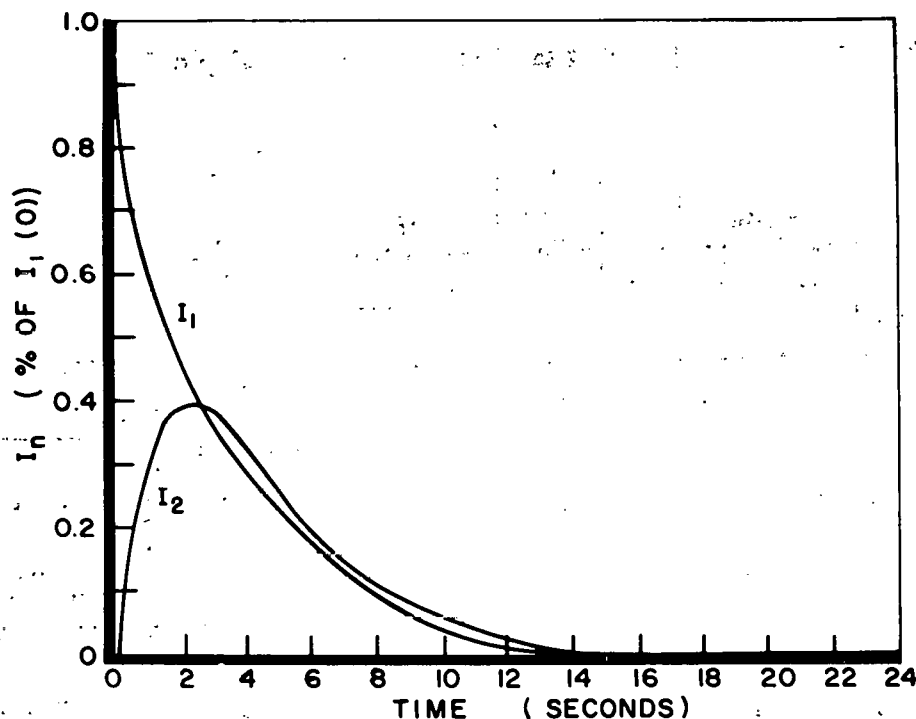
Fig. IV-7. The current-time response of the circuit in Fig. IV-5 which is analogous to the activities of the decay chain.

It should be noted that, due to the same mathematical form of $\sigma\phi$, the cross section flux product, and λ, the decay constant, it would be possible to calculate neutron activation problems analogically also.

H. Neutron Flux Measurements

The need for the further development of neutron measurement standards and techniques has become pressing. The determinations of absolute cross sections and the measurements of flux are closely interrelated from the measurement standpoint, and the general cross section program has now developed to the point that more precise flux values are greatly needed. To solve these problems methods must be expanded for differentiating between the various energy components of the reactor neutrons. The development and application of these techniques will greatly enhance the information that can be gained from various irradiation programs both internal to Phillips AED and external to the outside experimentalists.

Participation by the three MTR-ETR technical branches in these activities will increase. Efforts are being made to coordinate this work to serve the widest needs of Phillips and the AEC. The most immediate objective will be to increase the absolute accuracy of in-pile irradiations.

1. **Direct Fission Product Determination of the Amount of Fission**
(E. H. Turk, J. A. Dunbar)

Methods for measuring flux by determining the amount of fission by radiochemical determination of the Cs^{137} produced in the fission of U^{235} are being developed. In this approach a more direct comparison of heat and fission can be made.

2. **Au Resonance Integral Integrating Monitor** (E. H. Turk, J. A. Dunbar)

An integrating (total nvt) monitor is being developed for long term high flux irradiations. The Hg produced from Au activation is measured. In combination with the standard Co flux monitors, it is expected that an integral value for the resonance flux can be obtained. Thus, Au^{198} has a resonance integral cross section of about 15 times its thermal cross section while the resonance integral of Co is about equal to its thermal cross section. Thus, by a different method it is expected that an integral resonance flux can be measured without the flux depression which would accompany a cadmium-covered sample.

In this procedure the Au^{198} and its neutron capture products are allowed to decay to stable Hg which is then determined by chemical analysis. The method appears straightforward since second, third, and fourth order neutron capture in the Au all lead to isotopes decaying to stable Hg. Additionally, the Hg^{198} can itself capture up to four neutrons without producing any unstable isotopes of Hg.

I. IBM Machine Computational Facility

1. **General**

The volume of work done by the "650" has continued at a high level. In addition to regular (day shift) operations, 119 hours of overtime and scheduled second shift were used for machine computations. Processing of experimental and process-control data constituted a major fraction of the work. Also, 125 critical size and flux calculations were made.

The alphabetic device which enables the "650" to accept alphabetic as well as numeric information was installed. Also, the Electronic Associates Dataplotter, which automatically plots from cards, has been functioning very satisfactorily.

2. **Library Routines**

Programs written and/or checked out during this period include the following routines:

(a) Regression analysis from IBM

(b) Decay curve calculation

(c) Analysis of the dynamic behavior of the ETR

(d) Resonance escape probability computation

(e) Calculation of the atoms/cm^2 for various substances

(f) Conversion of octal numbers to decimal

(g) RAP, a routine obtained from IBM for calculating the constants and coefficients for a wide range of polynomial regression equations.

(h) A statistical interpretive system for the "650" obtained from IBM

(i) Computation of the dose (REM) to the critical organs

(j) Computation of xenon override

(k) Evaluation of specialized integrals

(l) Polynomial evaluation

(m) ETR power overshoot computations

(n) Calculations for fission break detection

(o) Transient heat transfer computation

(p) Computation of the accumulated dosage and cost of experiments in the gamma facility

(q) Calculation of the ETR charge life

(r) SOAP (Symbolic Optimal Assembly Program) obtained from IBM

(s) SIR (SOAP Interpretive Routine) obtained from IBM

(t) HOTCHA, a routine coded for NRF for sub-assembly thermo-hydraulic analysis

3. Machine Utilization

Operating statistics for the three months making up this quarter are given in the following table:

Month	Warm-up and Test-deck Time	Scheduled Maintenance	Unscheduled Maintenance	Power Failure	Production Time
January	2.31%	8.97%	4.09%	0.00%	84.63%
February	1.78%	9.02%	3.95%	0.10%	85.15%
March	0.91%	2.34%	3.01%	0.15%	93.59%

4. Production Time

     Of the 572.50 hours of production time in this quarter, 11.0% were spent in checking out programs, 89.0% in problem-solving and data reduction. A brief breakdown of the production time follows:

Data Reduction (Cross Sections)	32.67%
Data Reduction (SPERT)	15.49%
Data Reduction (ICPP)	3.90%
Data Reduction (Gamma-Ray Spectroscopy)	15.62%
Data Reduction (RMF)	2.08%
SPERT-I Theoretical Studies	4.48%
MTR "Technical Assistance" Calculations	11.10%
Theoretical Physics Computations	4.76%
Applied Mathematics Calculations	3.19%
Westinghouse (NRF)	6.71%

V. NUCLEAR PHYSICS

A. Cross Sections Program (R. G. Fluharty)

1. Cross Sections of U^{233} (M. S. Moore, C. W. Reich, O. D. Simpson)

The fission and total cross sections of U^{233} have been measured with the MTR fast chopper over the energy region 0.1 to 1,000 ev. The resolution for both measurements was 0.12 μsec/m, so that a meaningful total-minus-fission cross section could be obtained by direct subtraction. A consistent multilevel analysis has been made of these data, over the region of 0.1 to 12 ev. The parameters obtained are given in Table V-1. These results, combined with fission cross section data obtained on the MTR crystal spectrometer, are being prepared for publication.

TABLE V-1

Multilevel Parameters Obtained for U^{233}

E_o(ev)	Γ_n^o(mv)	g^*	Γ_γ	Γ_f
0.190	0.0006	7/12	0.044	0.080
1.75	0.178	7/12	0.044	0.080
2.32	0.086	7/12	0.036	0.048
3.61	0.057	7/12	0.054	0.180
5.75	0.040	7/12	0.050	0.320
6.79	0.300	7/12	0.050	0.146
9.05	0.021	7/12	0.056	0.280
10.33	0.410	7/12	0.070	0.274
1.47	0.140	5/12	0.040*	0.508
4.70	0.130	5/12	0.040*	0.650

*Assumed Values

2. U^{233} η Measurements (J. R. Smith, E. H. Magleby)

The Harwell U^{233} sample has been received and is being used in the measurement of the energy variation of η. In addition, samples of 0.030 inch and 0.170 inch thickness have arrived from Los Alamos, making possible a comparison of data on the basis of sample thickness. Measurements thus far in the current run cover the energy region from 0.025 ev to 3 ev, and will be extended to 10 ev or above. Modified "long" counters are being used as fission neutron detectors, with Cd and B_4C shields to screen out low energy neutrons scattered from the sample. Beam filters are being utilized to correct the data for effects due to neutrons from second order Bragg reflections in the crystal. This correction amounts to about 10% at thermal energy.

The new data appear to be considerably more self-consistent than the previous data obtained with the same sample. This is due primarily to the superiority of the new Be crystal over the NaCl crystal previously used. The superiority lies in the higher Bragg beam intensity and signal-to-noise ratio obtained with the Be crystal.

3. Fission Detector   (J. E. Cline)

Design studies have been made on a fission chamber which can effectively sort fission fragments from an intense background of gamma-rays, α particles, and β particles. Such a chamber must have a very fast response time, a linear energy response to α particles and fission fragments and a high counting efficiency.

A chamber has been designed which has these properties. The detection principle is that of a scintillation gas such as xenon with quartz window photomultiplier tubes. The chamber may be used as a coincidence chamber in which the fission fragments are detected in coincidence with each other. Construction of this system is about 20% complete.

4. Total Cross Sections   (F. B. Simpson, J. E. Cline, M. K. Brice)

The total cross section of Nd has been computed. The Nd measurements had to be redone to determine the effect of a special fuel element in front of the chopper beam hole during the previous measurements. The resonance parameters for the two even-odd isotopes from 1.0 to 200 ev have been determined. Total cross sections for Nd, Sm, Gd, and Pu^{240} were sent to Brookhaven for publication in a revision of BNL-325.

Work preliminary to measuring the total neutron cross section of Pd has been completed. Sample thicknesses have been calculated and appropriate samples have been ordered. In addition, enriched isotopes of Pd have been obtained from Oak Ridge National Laboratory for the purpose of identifying the resonances in Pd.

Total cross section measurements were made on two samples of Ir foil, from the thermal region up to ≈ 1 kev. Analysis of the data is in progress.

5. Scattering Cross Sections   (F. B. Simpson)

Scattering and total cross section measurements were made with the fast chopper on W, in order to determine the g values of the 27, 46, and 101 ev resonances. The g values found were 3/4, 1/4, and 1/4, respectively. A self-indication measurement was also made on this element to give some additional information in assigning the g values.

B. Inelastic Scattering of Slow Neutrons   (R. M. Brugger, L. W. McClellan, G. B. Streetman)

1. High Intensity Velocity Selector (Phased Choppers)

This program is being set up to measure the energy and angular distributions of neutrons scattered from reactor moderator and reflector materials as functions of incident neutron energy (below 1 ev) and material temperature. A high intensity velocity selector, which consists of two phased

choppers, is being installed at the HG-6 beam hole of the MTR. During this quarter, three rotor shells for the choppers were completed and delivered by Tools, Incorporated of Los Angeles. The insert foils for the rotors are being made at the MTR and are 70% complete. The vacuum tight rotor housings were assembled and aligned on the mounting table. The two Bekey motors that will turn the choppers at speeds of 1,000 to 15,000 rpm and three power amplifiers that will drive the motors were delivered. Spin and phasing tests of the rotor shells were starting at the end of the quarter. Two high pressure $B^{10}F_3$ counters were delivered by RCL and tests were started to determine their appropriateness for this experiment. A remote-activated, motor-driven gate drive system for the HG-6 beam hole plug was installed. A contamination shielding pan to cover the HG-6 beam hole area was designed and construction started.

2. Spinning Sample Experiment

In order to gain practical experience, preliminary survey measurements with beryllium-filtered neutrons are being made by a new technique. Bursts of scattered neutrons are provided by a sample attached to a motor-driven rotating arm. When available, the fast chopper 1024 channel analyzer is used for time-of-flight measurements on the scattered neutrons. In addition to the simplicity of this method, there is no time dependent background due to neutrons scattered from the sample between bursts.

Fig. V-1 shows the arrangement of equipment for the spinning sample experiment. Initially, the sample (5) was contained in a 3 inch long, 1/8 inch I.D. aluminum can. This can was mounted 15 inches from the center of rotation of the arm and the detectors were 80 inches from the beam. Fig. V-2 shows the data taken with a water sample with elastically scattered neutrons at 2,200 μsec, and a hump at 1,000 μsec and a peak near thermal, due to inelastically scattered neutrons. The data agree with those obtained by Brockhouse[19] except that we are observing multiple scattering effects because of a thick sample. The statistics are poor since the 1024 channel analyzer was available only for two hours and sufficient data for good statistics could not be accumulated. Modifications have been made to suppress the background and multiple scattering effects and to improve the resolution. When a time analyzer becomes available, these experiments will be continued.

C. Nuclear Chemistry Program (W. H. Burgus)

1. Mass Yields in the Resonance Fission of U^{233} (R. B. Regier, R. L. Tromp, W. H. Burgus)

Measurements were continued in which the "peak to trough" mass yield ratios were compared for resonance fission and for thermal fission of U^{233}. Additional thermal irradiations of U^{233} were made in the VG-23 facility of the MTR to obtain ratios of the saturated counting rates of Mo^{99}/Ag^{111}, Mo^{99}/Ag^{113}, and Mo^{99}/Cd^{115}. These empirically determined counting ratios for thermal fission provide the reference values with which the same ratios for resonance fission are compared. The precision attained to date in measuring the thermal Mo^{99}/Ag^{111} and Mo^{99}/Cd^{115} ratios has not been as good as might

(19) B. N. Brockhouse, Structural Dynamics of Water by Neutron Spectrometry, Supplemento del Nuovo Cimento, (Proceedings of the Varenna Conference on the Condensed State of Simple Systems), Acta. Cryst. 10, 827, (1957).

1. DETECTORS
2. MAGNETIC PICKUP
3. DEFINING SLITS FOR
      SCATTERED NEUTRONS
4. BEAM-CATCHER TANK
5. SPINNING SAMPLE
6. MOTOR
7. REACTOR SHIELDING FACE
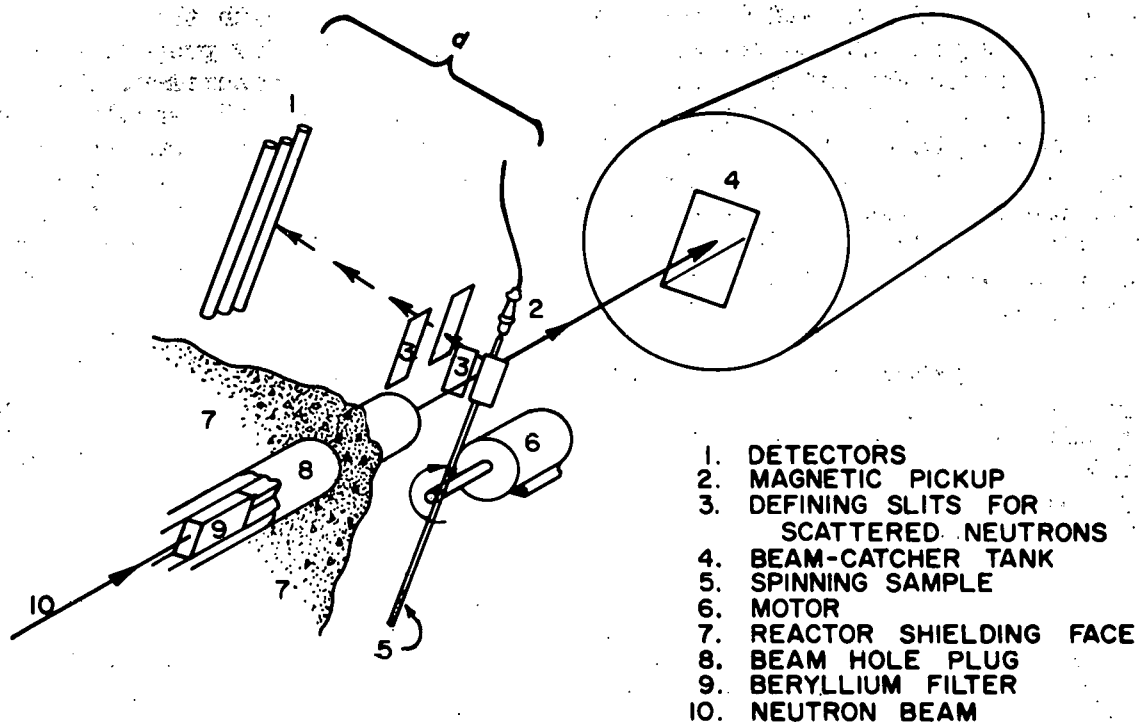8. BEAM HOLE PLUG
9. BERYLLIUM FILTER
10. NEUTRON BEAM

Fig. V-1. A schematic deagram of the spinning sample experimental setup.
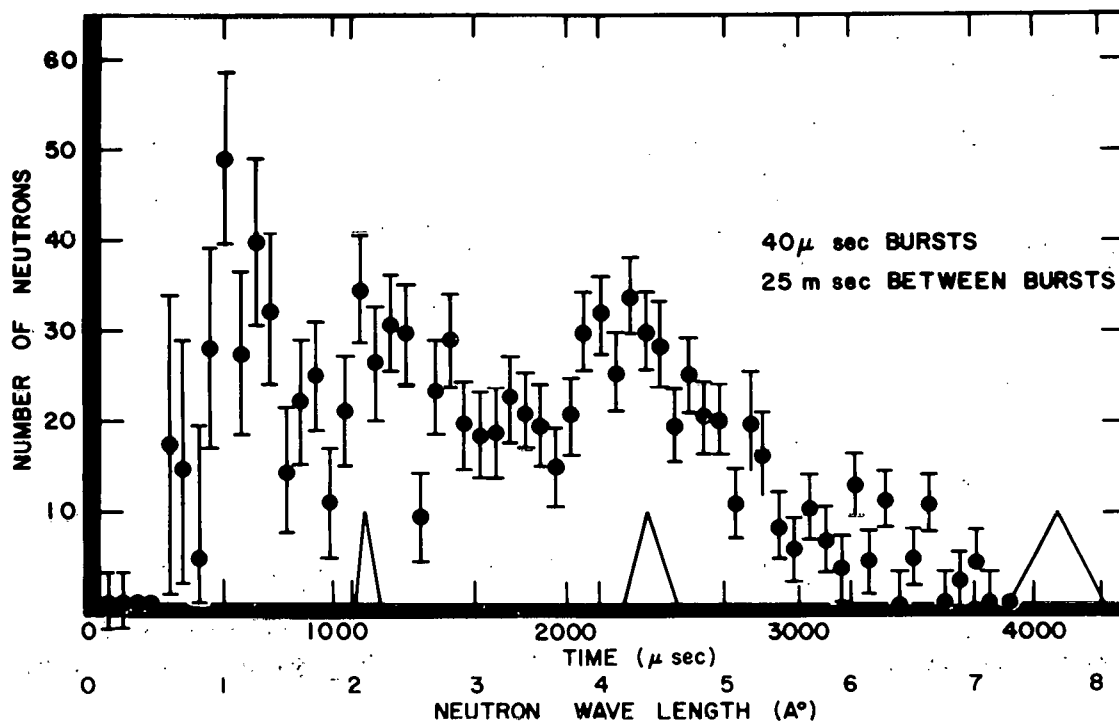The motor operates at about 1,200 rpm.

Fig. V-2. The wave length spectrum of Be-filtered neutrons scattered at 90°
from H_2O. Elastically scattered neutrons have wave lengths of 4 angstroms
or greater.

be desired. The Ag and Cd samples have been counted with the low-background counting equipment and the Mo samples with an end-window proportional counter since the latter samples are too active for measurement with the Geiger counters employed in the low-background system. It should be pointed out that although the counting efficiencies of the two systems are different, this in no way invalidates the comparisons made between resonance and thermal fission since the counting efficiency of a counter for a given radioactive nuclide is independent of whether that nuclide originated in resonance or in thermal fission. Experiments to improve the thermal fission data are continuing.

A number of resonance neutron irradiations were also made during the quarter, using neutrons from the Bragg beam of the crystal spectrometer. In addition, a series of irradiations of cadmium-covered U^{233} samples was made in MTR positions where there is appreciable fast neutron flux. These irradiations provided neutrons for fission above the Cd cutoff and freed the spectrometer for other experiments.

A summary of the results obtained during this quarter is given in Table V-2. The values quoted are based on seven thermal irradiations in VG-23, four spectrometer irradiations at 2.3 ev and two spectrometer irradiations at 4.7 ev. Also included are the results from four samples covered with 0.020" Cd, three of which were irradiated in the VG-7 facility, and one in the VH-1 facility. Although the epi-cadmium spectra are recognized to be different in these two positions, the results of the four cadmium-covered experiments have been grouped together. The uncertainties associated with the values given in Table V-2 are based upon the variations between the individual determinations and are expressed as the standard error, σ.

TABLE V-2

Comparison of Resonance and Thermal Mass Yield Ratios

Neutron Energy	$\left[\dfrac{Mo^{99}/Ag^{111} \text{ (resonance)}}{Mo^{99}/Ag^{111} \text{ (thermal)}}\right]$	$\left[\dfrac{Mo^{99}/Cd^{115} \text{ (resonance)}}{Mo^{99}/Cd^{115} \text{ (thermal)}}\right]$
2.3 ev	1.05 ± 0.03	1.09 ± 0.10
4.7 ev	0.88 ± 0.04	0.76 ± 0.05
All epi-Cd	1.09 ± 0.05	1.20 ± 0.07

From the data of Table V-2 it is clear that the difference in the "peak to trough" ratio between resonance and thermal fission is not large. This had been indicated by work of the previous quarter[20] in which it was shown that the Mo^{99}/Ag^{111} ratio was larger by $15 \pm 3\%$ for 1.8 ev fission

(20) R. B. Regier and W. H. Burgus, Quarterly Progress Report for MTR-ETR Technical Branches, Fourth Quarter - 1957, IDO-16436, 56.

than for thermal fission of U^{233}. The difference between the results for the 1.8 ev and 2.3 ev resonances can be explained by the relative amounts of non-resonance fission contributions resulting from the energy spread of the neutrons in the Bragg beam. The results reported in Table V-2 for 4.7 ev resonance irradiations are questionable because of the possibility that the U^{233} sample was partly in the main beam of the spectrometer as well as in the 4.7 ev resolved beam. However, the result obtained is very interesting in view of the fact that the main beam emerging from the reactor passes through a 0.040" Cd filter before reaching the spectrometer and thus any portion of the sample that was in the main beam was not subject to a high thermal flux. A weak low energy component may have been present however, due to scattered neutrons. Use of cadmium-covered samples for spectrometer irradiations will help to eliminate the effects of any low energy neutrons. Because the Mo^{99}/Ag^{111} ratio obtained at 4.7 ev is less than that obtained in thermal irradiations, further spectrometer irradiations at this and at other energies are planned for the next quarter in an effort to improve the precision and reliability of the measurements.

2. Second Order Capture Studies (E. H. Turk, R. P. Schuman)

Irradiations of Co are continuing, to obtain better information on the capture cross section of Co^{60}.

A sample of Re metal was irradiated at about 2×10^{14} neuts/cm^2 sec for a total nvt of about 1.4×10^{21} neuts/cm^2 in an attempt to measure the capture cross section of Re^{188} and to produce a sufficient quantity of Re^{189} for decay scheme measurements. The presence of an overwhelming amount of Re^{188} has thus far masked any Re^{189} that has been formed and the sample must be allowed to decay further before any Re^{189} measurements can be attempted.

3. Heavy Element Studies (R. P. Schuman)

In order to prepare a high purity U^{236} sample for thermal fission cross section measurements on U^{237}, long pile irradiation of two samples of U, enriched in U^{236}, has been started. The samples are being irradiated in order to burn out the bulk of the residual U^{235}. Samples of Co and Mn are being irradiated with the U samples in order to monitor the integrated flux. The Mn capture will be determined by chemically analyzing for the Fe produced.

Calculations of the production of Np^{237} and Pu^{238} in MTR irradiated fuel have been made in order to evaluate the irradiated fuel as a source of Np^{237}. A considerable fraction of the neutron capture of U^{236} in a reactor is due to resonance neutrons; consequently the calculations of Np^{237} production are uncertain because of the poorly known reactor resonance flux and the resonance integral for U^{236}. A resonance integral of 310 barns was calculated for U^{236} from the resonance parameters.[21] This value is in fair agreement with the value of 257 ± 22 barns measured at Chalk River.[22]

---

(21) D. J. Hughes and R. B. Schwartz, Neutron Cross Sections, Supplement No. 1, BNL-325, (1957).

(22) T. A. Eastwood, private communication.

The calculated production of Np^{237} in irradiated fuel (~300 mg per kg of U for 29% burnup) was in fair agreement with the amount determined chemically at ICPP. The production of Np^{237} and Pu^{238} are not very flux dependent for the fluxes available in the MTR.

4. Counting Equipment Development (R. P. Schuman)

A graphite back to back in-pile fission chamber is being built for the measurement of thermal fission cross sections for heavy isotopes. The electronics components for fission counting have been received and are being tested by counting the spontaneous fission of Cf^{252} in a brass fission chamber built for spontaneous fission experiments.

A Tracerlab Frisch grid alpha ionization chamber has been received and will be used with the counting room 256 channel analyzer for alpha energy determinations.

5. Short-Lived Fission Product Studies (R. P. Schuman, E. H. Turk, R. L. Heath)

The study of the decay scheme of La^{142} has continued. Some preliminary gamma-gamma coincidence measurements have been made with ambiguous results. Additional measurements are planned. The decay scheme is very complicated and only part of the Ce^{142} levels will be determined in the present work.

D. Decay Schemes and Nuclear Isomerisms

1. Scintillation Detector Calculations (S. H. Vegors, R. L. Heath)

Calculations of the efficiency of right cylindrical NaI(Tl) scintillation detectors for extended sources of radiation have now been completed. The two cases considered were (A) a disk source of radiation centered on the extended central axis of the detector with the plane of the disk perpendicular to this axis and (B) a line source of radiation perpendicular to the extended central axis of the detector with the center of the line source being on this axis.

Results for the disk source case, A, were obtained for five values of the source detector distance, h, (h = 0.001, 1, 3, 5, and 10 cm). Values used for the radius of the disk were 0.250, 0.500, 0.750, and 0.999 of the radius of the cylindrical detector. Calculations were made for three crystal sizes, 3" dia x 3" thick, 1 3/4" dia x 2" thick, and 1 1/2" dia x 1" thick. Results were obtained for ten values of τ (gamma-ray absorption cross section in cm^{-1}) covering a range of gamma-ray energies from 30 kev to 5.5 Mev.

Calculations for the line source case, B, were made for the same detector sizes for the same range of gamma-ray energy as were used in case A. However, calculations were performed for only three values of source-detector distance, namely h = 0.001, 1, and 5 cm. The lengths of the line sources considered were 0.250, 0.500, 0.750, and 0.999 of the diameter of the detector.

The above results plus those obtained for similar, but much more extensive, calculations for a point source of radiation appear in a published report.[23]

2. A 4.7 Millisecond Isomer in Pb^{205} Formed by the Decay of Bi^{205}
(S. H. Vegors, R. L. Heath)

In the course of the present investigation of the electron capture decay of Bi^{205} it was noted that one of the major transitions, the 987 kev gamma-ray, was not in prompt coincidence with the electron capture x-rays. Since previous data had shown that this gamma-ray was not in coincidence with any of the other gamma-rays associated with the decay of Bi^{205}, it became apparent that the 987 kev transition might very well come from the decay of an isomeric level.

In order to look directly at the spectrum of the gamma-rays which were not in coincidence with the electron capture x-rays, the following experiment was performed. A source of Bi^{205} was placed in the center of a 1/4 inch thick split crystal as is shown in Fig. V-3. The output pulses from the split crystal which is sensitive only to x-rays (having an efficiency of >95% for the detection of the Pb K x-ray) was fed to an anticoincidence circuit. This circuit gated off the multichannel pulse height analyzer for all gamma-rays entering the 3" x 3" crystal which were in prompt coincidence with the x-rays with a resolution of 0.3 μsec.
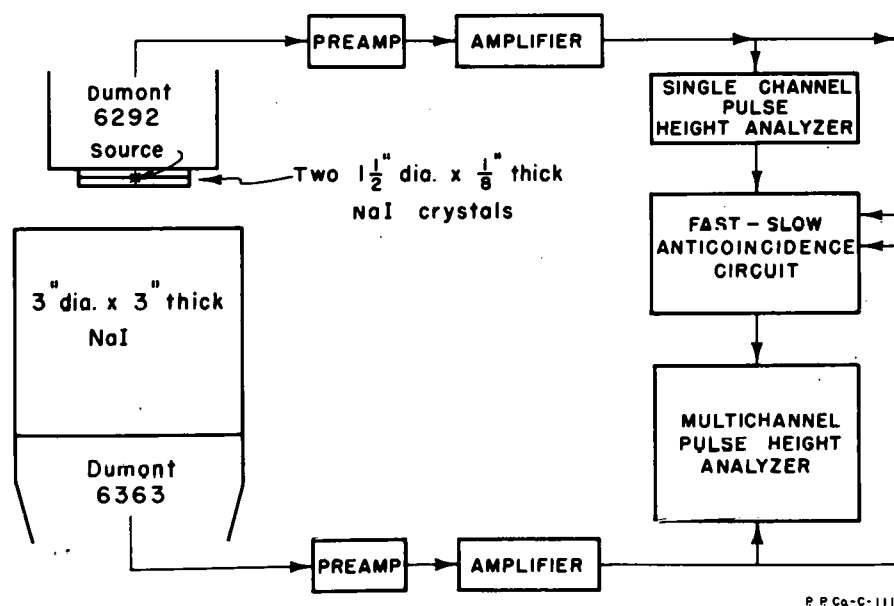

Fig. V-3. Experimental arrangement used to demonstrate the existence of an isomeric state in Bi^{205}.

---

(23) S. H. Vegors, L. L. Marsden, R. L. Heath, Calculated Efficiencies of Cylindrical Radiation Detectors, IDO-16370, (1958).

The result of this measurement is shown in Fig. V-4. This plot
shows a comparison between the gamma-ray spectra obtained on the 3 inches
in diameter by 3 inches high detector with and without the anticoincidence
requirement. The strong enhancement of the 987 kev peak indicates that this
gamma-ray is not in prompt coincidence with the electron-capture x-rays.
From this it was concluded that this gamma-ray arises from a delayed state.
The slight enhancement of the 569 kev gamma-ray results from the presence
of the 0.8 sec Pb^{207} isomer as a contaminant. Further investigation using
a well crystal substantiated the hypothesis that the 987 kev level in Pb^{205}
is isomeric. Its half-life was measured by counting the number of gamma-
rays in a 60 kev window centered on the 987 kev gamma-ray using the Pb K
x-ray to mark the time t = 0. The result of these measurements gave a half-
life of 4.7 $\pm$ 1.5 milliseconds for the 987 kev level in Pb^{205}.

3. Multichannel Pulse Height Analyzer Storage System Design (R. I. Little, A. W. Magnuson)

The storage system for the multichannel pulse height analyzer
(transistorized) must be able to store pulses separated by as little as 2.4
μsec, and where the average pulse rate will be 30,000 counts per second the
pulse count loss due to the storage system is to be of the order of 0.1% or
less.

Since the proposed permanent storage magnetic core takes approximately
20 μsec to complete storage of a pulse reliably, and since the probability of
more pulses occurring during the storage interval is high, a system of
temporary storage currently under development will be utilized. If this
storage system is clear of data initially, it accommodates temporarily four
pulses in slightly less than 10 μsec, 5 in 20 μsec, 6 in 40 μsec, and another
for each 20 μsec elapsed time. The ability of the temporary storage system
to store up to four pulses in rapid order practically eliminates the counting
loss.

The prototype for this system, shown in Fig. V-5, employs only 16
inputs, adequate for checking its feasibility. The final version will employ
six groups of 24 inputs, and will be capable of being enlarged to eight
groups of 32 inputs. These inputs will first be encoded into the binary
system by use of diode encoder groups. Pulses passing through the encoders
determine the states of four flip-flops. This yields 2^4 combinations to
gate four "half-current" generators. These generators feed the horizontal
lines of a magnetic core matrix with just half enough current to "flip"
the cores.

The "write" address scaler selects, in rotation, the one vertical
storage line of four on which input pulse information is temporarily stored.
Any time an input pulse arrives, a coincident "total count" trigger switches
a "write" pulse on, and 2 μsec later switches it off again. The "write"
pulse drives a half-current generator on the vertical storage line which
was selected by the "write" address scaler. The same trigger which terminates
the "write" pulse also resets all the input flip-flops, thus switching off
their half-current generators. This trigger also advances the "write"
address scaler and starts the permanent storage sequence. Any core subject
to half-current pulses coincidently on both horizontal and vertical lines
now has been "flipped", and when subject to a pulse of opposite polarity
will yield a small, but usable output voltage on any coincident conductor.
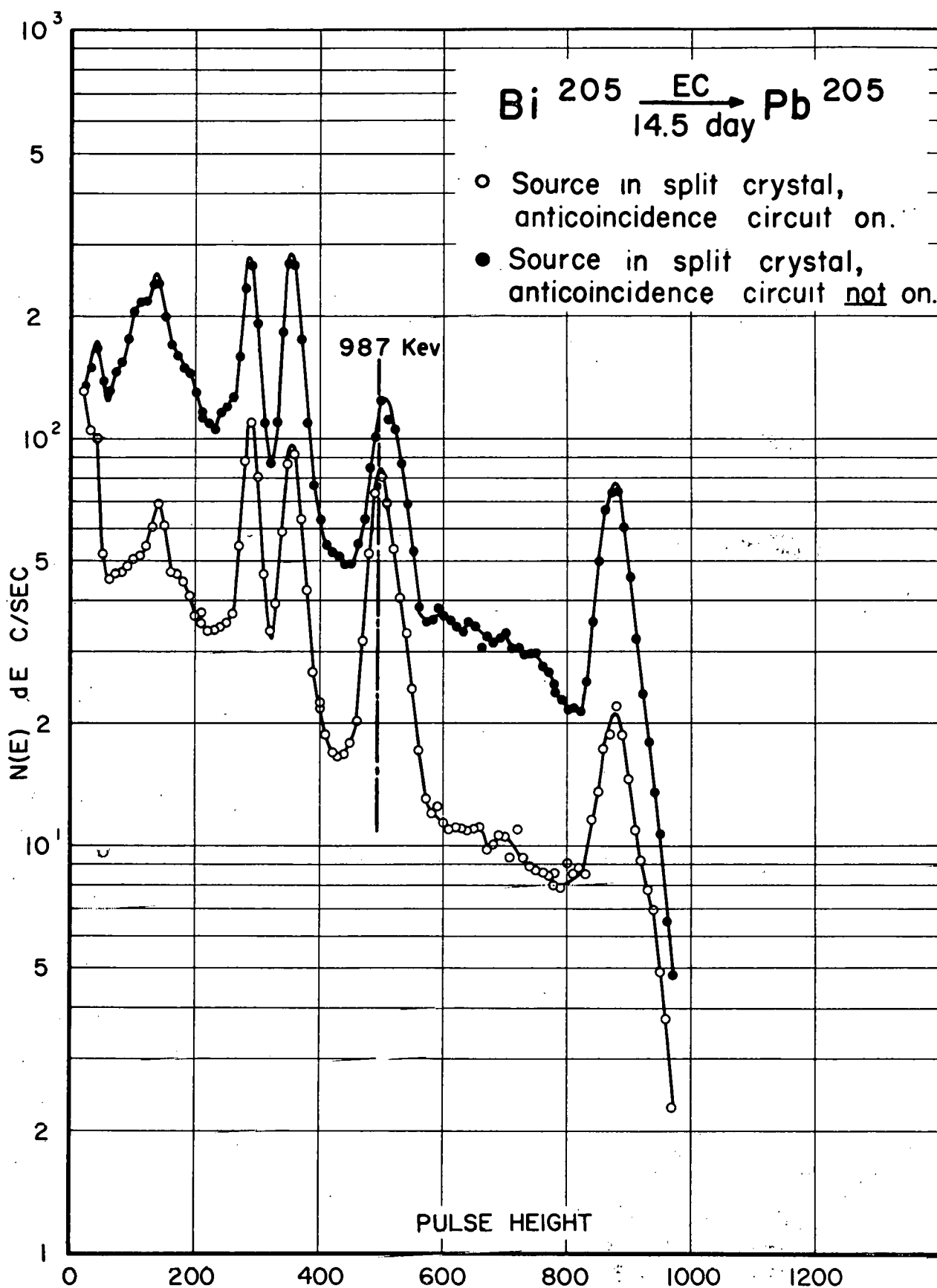
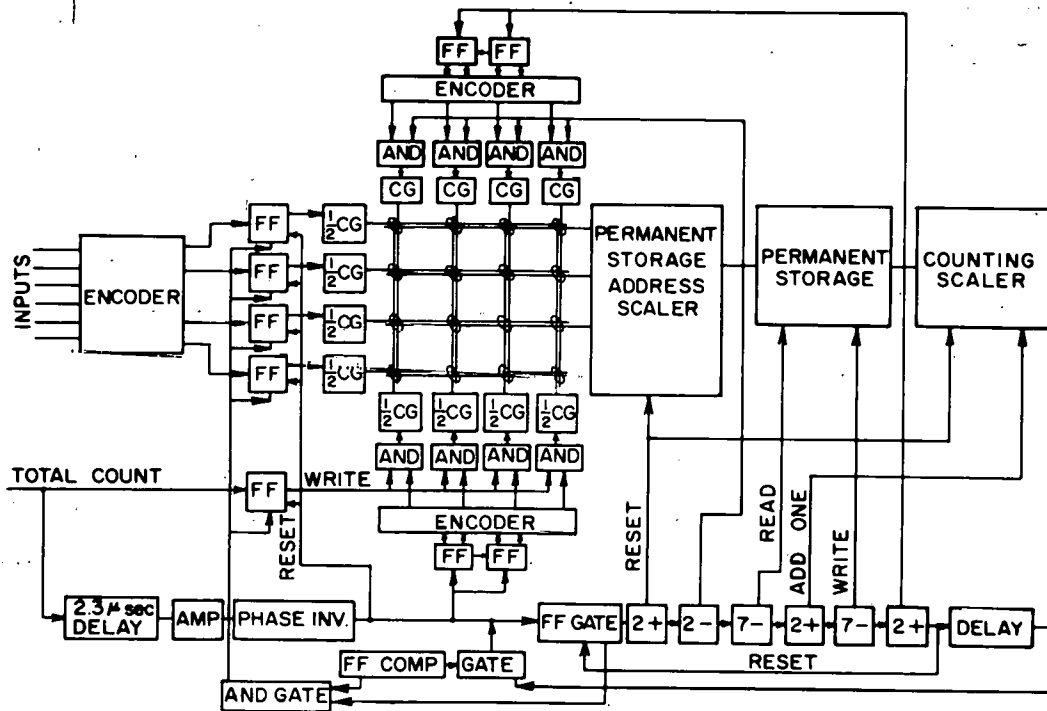Fig. V-4. Gamma spectrum, with and without anticoincidence circuit.

Fig. V-5. Multichannel pulse height analyzer prototype storage system.

Any time the temporary storage matrix is empty and receives a pulse, the permanent storage system immediately starts storing this pulse. Since it takes 20 μsec to store a pulse, when the permanent storage cycle has finished, the temporary storage unit may or may not have more pulses to store. If not, the permanent storage system will await the next incoming pulse. If in the meantime the temporary matrix stores more pulses, the permanent storage system cycles until it has "caught up".

A "read" address scaler similar to the "write" address scaler selects the vertical line from which temporarily stored data is read out. A pulse furnished by the permanent storage sequencer drives the full current generator thus selected, and the voltages thus induced appear on the horizontal output lines opposite the respective cores. The full current generator adequately resets the cores.

The horizontal output lines terminate in independent amplifiers which in turn precede a permanent address scaler which determines the exact channel in the permanent storage system to which the count is added.

The permanent storage matrix consists of a 12 x 12 x 16 array of magnetic cores. A 12 x 12 plane yields 144 channels, and the depth of 16 cores allows 2^{16} or 65,536 pulse counts to be stored in each channel.

When a pulse is to be permanently stored, first the address scaler selects the proper channel, then the sequencer reads out the existing count into a counting scaler, simultaneously resetting the cores in the selected channel. Next the sequencer adds a count of one (representing the "one" pulse which is being stored) to the counting scaler, and then the sequencer furnishes drive to write the new total back into the same channel of the permanent storage.

The permanent storage sequencer consists of a chain of one-shot multivibrators which are preceded by a sequencer gate. When triggered, this multivibrator chain will complete automatically a permanent storage sequence. This consists of:

(1) Resetting of the permanent address and the arithmetic scaler with a 2 μsec pulse.

(2) Furnishing the 2 μsec pulse necessary to read out and reset one vertical storage line in the temporary storage matrix, to set the permanent address scaler.

(3) Driving permanent storage readout with a 7 μsec pulse.

(4) Pulsing the counting scaler with a 2 μsec "add one" pulse.

(5) Writing into magnetic storage the new count with a 7 μsec pulse.

(6) Furnishing a trigger pulse. This trigger advances the "read" address scaler in the temporary system to the next vertical storage line and resets the sequencer gate. It also undergoes a 1 μsec delay after which it is available again to trigger the sequencer gate if necessary.

Normally the temporary "read" address scaler catches up to the "write" address scaler in the absence of input pulses. A comparator determines that they are in the same state and gates off the delayed trigger to the sequencer gate. If more pulses have been temporarily stored since the beginning of the last sequencing cycle, the "write" address scaler will have advanced, and the indication of difference presented by the comparator gate will allow the delayed trigger to recycle the sequencer.

A gate which can cut off all inputs will close whenever the sequencer gate is closed (indicating permanent storage is taking place) and the scaler comparator indicates sameness. This condition can only come about when the temporary "write" address has stored four more pulses than have been permanently stored. Further pulse storage would result in two pulses being stored on the same vertical address line and when read into permanent storage would lead to erroneous data accumulation. The gate will open as soon as a storage cycle is complete, thereby leaving one vertical line available in temporary storage as soon as possible.

The temporary storage system, accommodating 16 inputs, is complete in prototype but an incomplete output system prohibits thorough evaluation at present.

VI. PAPERS AND PUBLICATIONS

A. Journal Publications

1. K. A. McCollom, D. R. deBoisblanc, J. B. Thompson, *Sensitive Measurement of Pulse-Amplifier Gain*, Nucleonics, 16, No. 1, 74-8, January 1958.

B. IDO Reports Issued

IDO No.	Title	Authors
16435	Engineering Test Reactor Critical Facility Hazard Summary Report Supplement I	D. R. deBoisblanc E. E. Burdick T. K. DeBoer
16440	Spherical Harmonic Methods in Slab Geometry	D. R. Metcalf G. A. Cazier
16443	An Estimate of the Heat Generation and Distribution in the MTR	R. A. Grimesey
16449	A Multilevel Formula for the Fission Process	C. W. Reich M. S. Moore

C. Papers Presented at Meetings

1. Papers Presented at the Annual Meeting of The American Physical Society in New York, January 29 - February 1, 1958.

   a. R. B. Regier, W. H. Burgus, J. R. Smith, and M. S. Moore, *Neutron Energy Dependent Mass Distribution in U^{233} Fission.*

   b. E. H. Magleby, *Total Neutron Cross Section Measurements of Ca, Sr, Na, and K.*